Automated Implementation of the Edinburgh Visual Gait Score (EVGS)

Shri Harini Ramesh

Thesis submitted to the Faculty of Engineering
in partial fulfillment of requirements for the degree of

Master of Applied Science

in

Biomedical Engineering

Ottawa Carleton Institute for Biomedical Engineering
University of Ottawa

Ottawa, Ontario

Abstract

Analyzing a person's gait is important in determining their physical and neurological health. However, typical motion analysis laboratories are only in urban specialty care facilities and can be expensive due to the specialized personnel and technology needed for these examinations. Many patients, especially those who reside in underdeveloped or isolated locations, find it impractical to go to such facilities. With the help of recent developments in high-performance computing and artificial intelligence models, it is now feasible to evaluate human movement using digital video. Over the past 20 years, various visual gait analysis tools and scales have been developed. A study of the literature and discussions with physicians who are domain experts revealed that the Edinburgh Visual Gait Score (EVGS) is one of the most effective scales currently available. Clinical implementations of EVGS currently rely on human scoring of videos.

In this thesis, an algorithmic implementation of EVGS scoring based on hand-held smart phone video was implemented. Walking gait was recorded using a handheld smartphone at 60Hz as participants walked along a hallway. Body keypoints representing joints and limb segments were then identified using the OpenPose - Body 25 pose estimation model. A new algorithm was developed to identify foot events and strides from the keypoints and determine EVGS parameters at relevant strides. The stride identification results were compared with ground truth foot events that were manually labeled through direct observation, and the EVGS results were compared with evaluations by human scorers.

Stride detection was accurate within 2 to 5 frames. The level of agreement between the scorers and the algorithmic EVGS score was strong for 14 of 17 parameters. The algorithm EVGS results were highly correlated to scorers' scores ($r>0.80$) for eight of the 17 factors. Smartphone-based remote motion analysis with automated implementation of the EVGS may be employed in a patient's neighborhood, eliminating the need to travel. These results demonstrated the viability of automated EVGS for remote human motion analysis.

Table of Contents

List of Figures

List of Tables

Abbreviations and Definitions

AI	Artificial Intelligence
2D	Two-Dimensional
EVGS	Edinburgh Visual Gait Scale
PD	Parkinson's Disease
MS	Multiple Sclerosis
CP	Cerebral Palsy
IGA	Instrumented Gait Analysis
VGA	Visual Gait Analysis
PRS	Physician Rating Scale
SF-GT	Salford Gait Tool
OGA	Observational Gait Analysis
OGS	Observational Gait Scale
VGAS	Visual Gait Assessment Scale
SCP	Spastic Cerebral Palsy
CNN	Convolutional Neural Network
RAM	Random Access Memory
GPU	Graphics Processing Machine
FLIC	Frames Labelled In Cinema
LSP	Leeds Sports Pose
CUDA	Compute Unified Device Architecture
PAF	Part Affinity Field
ASIS	Anterior Superior Ilac Spine
KPA	Knee Progression Angle

Acknowledgements

First, I sincerely thank and appreciate my supervisors, Prof. Natalie Baddour and Prof. Edward Lemaire, for believing in me and allowing me to work at the Mobile motion lab. I could not have completed my thesis without their informative guidance, encouragement, and patience. They supported me every week, even when research progress was slow, and they were there for me at every research stage. They assisted me in being more organized and showed me how to think like a researcher while solving problems. And without the continuous assistance of CHEO doctors Dr. Albert Tu and Dr. Kevin Cheung, who contributed their vast clinical and EVGS-related knowledge, this research would not have been possible.

The greatest gratitude goes to my family, especially my parents, Ramesh Narayanan, and Nithya Jayalakshmi Ramesh, my brother Shri Vignesh Ramesh, and my sister-in-law Kamakshi Shri Vignesh. Their help, guidance, and, most importantly, their unconditional love have always inspired me to express myself more clearly and accomplish all my goals. I am eternally grateful for everything they have done and continue to do for me. I am also grateful to my late grandmother, Janaki, for her unwavering support throughout my academic journey. Her encouragement to pursue higher education and pursue my career goals gave me the drive to complete my thesis despite the challenges. I dedicate this thesis to her memory, with deep appreciation for the role she played in my life.

This thesis is part of the CREATE-BEST program funded by the Natural Sciences and Engineering Research Council of Canada (NSERC); my sincere acknowledgments for financing this research.

Finally, I'd like to thank all my friends and colleagues at The University of Ottawa, Ottawa Hospital Rehabilitation Centre, and The Children's Hospital of Eastern Ontario for their help with data collection and validation.

1 Introduction

1.1 Research context and scope

Gait is a complex activity requiring the coordination of several body systems and parts [1]. The process of evaluating kinetic, kinematic, and spatial-temporal characteristics in people with both normal and impaired walking is called gait analysis. On a clinical level, gait analysis is often used with people suffering from neurological disorders or orthopedic problems, providing objective information for clinicians when developing recovery plans or gait prevention programs [2].

Gait analysis laboratories use cameras and markers placed on key anatomical areas and limbs to accurately track a person's movement [3]. However, various drawbacks include time to obtain and analyze data, cost, and the need for trained professionals. These gold standard systems are mostly found in major urban areas. Due to restricted transit options and people's mobility, in addition to high system costs, instrumented gait analysis is not widely available, in particular for people in isolated or remote places [4].

Recent advancements in video-based pose estimation algorithms have made it possible to analyze human movement using digital video [5]–[8]. Numerous visual gait assessment tools [9], [10] or scales have been created over the last two decades [11]–[15] for neurological disorders such as Parkinson's disease (PD), Multiple Sclerosis (MS), Cerebral Palsy (CP), and stroke, which are some of the most prevalent pathologies influencing gait.

Pose estimating models have great potential to increase access to gait analysis for patients and video-based data collection can be carried out in a convenient location with minimal equipment. This would offer a preliminary gait interpretation and allow medical professionals to choose which patients would benefit the most from a more-thorough investigation and which patients could be postponed since their status had not changed.

1.2 Rationale

Human gait analysis is an important measure of a person's physical and neurological health. The analysis can be conducted with full 3D instrumented gait lab studies or observational assessments. However, patients hay have difficulty attending motion labs or seeing experienced observational gait analysis clinicians. This is especially difficult for children with mobility issues, where parents

need to take time off work and arrange care for other children. Winter conditions can also make travel to medical appointments unsafe. Smartphones have become ubiquitous and can greatly benefit gait monitoring, with the potential to replace or augment expensive medical technology since they are portable, lightweight, and comparatively inexpensive while also providing a high-quality video recording of human movement. Artificial Intelligence (AI) algorithms can use smartphone video for pose estimation, locating a person's joints in an image or video.

The Edinburgh Visual Gait Score (EVGS) has emerged as a reliable option for grading patient walking videos, particularly for children with cerebral palsy . The clinician visually evaluates a video and provides scores for various aspects of walking biomechanics, which can be used to assess the child's current movement status and also compare walking before and after an intervention. EVGS requires human assistance and can take a more time than available to implement. Each trial can take more than 20 minutes of grade [16]. To address these limitations, there is a need to combine existing technologies and develop new algorithms to provide automated EVGS analysis of smartphone video clips. This would enable gait analysis from any location, including rural clinics. This thesis aims to design and develop a system that can automatically use locally recorded smartphone videos and automatically perform EVGS analysis with minimal human interaction for scoring.

1.3 Scope

This research is for people requiring visual gait analysis. Since the EVGS was developed and validated for children with CP (i.e., ranges and values in EVGS are related to CP population), the scope for this research is limited to this population. However, this approach used in this thesis should be applicable to other groups with validated scales based on video analysis.

1.4 Objective

Design and evaluate an algorithm for detecting foot events and strides, and automatically determine the Edinburgh Visual Gait Score (EVGS) from video obtained with a handheld smartphone camera.

1.5 Thesis contributions

The thesis is novel in this domain since the automated implementation of scale-based visual gait analysis using smartphone data has never been developed and verified. This thesis has made

substantial contributions to the field of remote visual gait analysis technology and knowledge, including:

- Creation of a viable system that can detect foot events and strides and automatically score EVGS using a smartphone. This contribution was achieved through the design, development, and analysis of the system, and provides a basis for integrating automatic EVGS analysis and scoring using smartphones in an individual's preferred environment.
- Demonstration that most EVGS parameters can be obtained using Openpose keypoints alone, without requiring any markers or gait analysis systems . However, certain parameters lack machine-friendly thresholds or cannot be directly obtained from OpenPose keypoints. In such cases, surrogate measures were introduced as alternative approaches for estimating these parameters.
- The proposed automatic system is time-efficient and can potentially reduce the workload for clinicians. Unlike the manual EVGS scoring process, which takes an average of 24.7 minutes after video recording [16], the new approach can provide EVGS scores quickly and automatically without the need for manual calculations or human intervention.

Overall, this thesis presents a novel and time-efficient method for calculating EVGS scores using smartphone video data, which has potential clinical applications in remote visual gait analysis technology. The contributions also advance the understanding of automatic gait analysis methods using EVGS and provide a basis for future research in this area.

1.6 Thesis outline

Chapter 2 is a literature review that discusses gait biomechanics, current methods of gait analysis, covering various scales in observational gait analysis, and deep learning models for human pose estimation.

Chapter 3 introduces and explains the Edinburgh Visual Gait Scale (EVGS) analysis.

Chapter 4 presents the algorithmic implementation of the EVGS. The steps involved in analyzing human gait using the EVGS, including the automated detection of strides in videos, are presented.

Chapter 5 presents the methods and results for evaluating the proposed algorithmic implementation, including collecting data.

Chapter 6 summarizes and concludes the thesis.

2 Literature Review

2.1 Gait biomechanics

Walking requires a complex interaction of forces exerted by muscles on bones, rotations across several joints, and external forces acting on the body [17]. Gait analysis studies human movement, and the gait cycle is used to define the repeating walking period [18]. The gait cycle has been classified into stance and swing phases, periods, and events to allow the identification and separation of distinct parts [19] (Figure 2.1).

A gait cycle starts with a foot strike and finishes with another foot strike on the same side [20]. Foot strike and foot off are events and loading response, mid-stance, terminal stance, pre-swing, mid-swing, and terminal swing are periods in a typical gait cycle. Each gait cycle is divided into stance and swing phases. Stance phase lasts from foot strike to toe-off, accounting for approximately 62% of the gait cycle. Swing phase begins with a toe-off and finishes with a foot strike, accounting for 38% of the cycle [21].

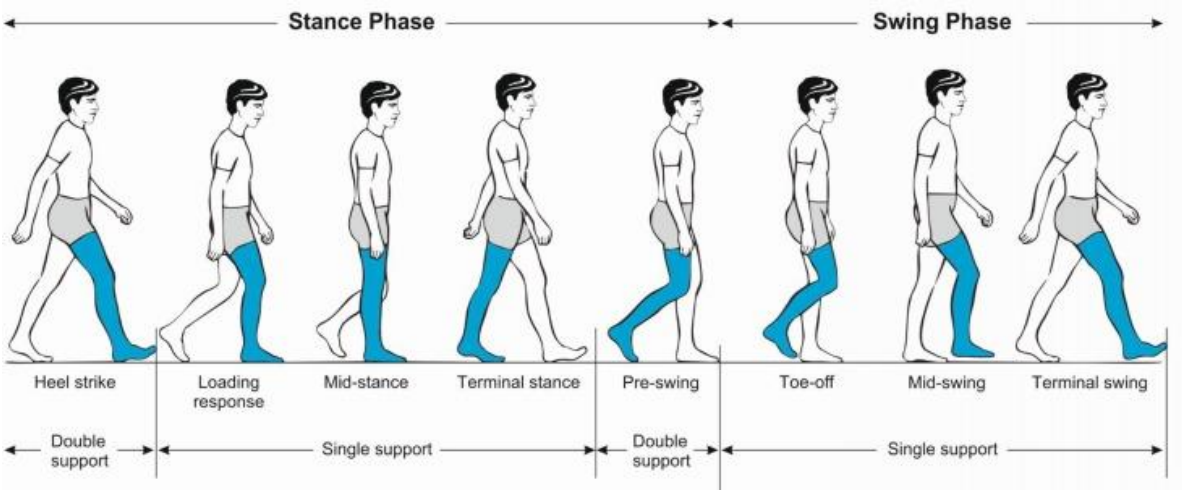

Figure 2.1 Gait cycle [19]

2.1.1 Stance phase

Stance phase starts when the foot touches the ground and begins to support body weight. The body proceeds over the stance leg and provides shock absorption for the entire body. Stance phase can be divided into five periods [22]–[24].

- Heel strike: Occurs when the foot contacts the ground and receives body weight and ends

when the contralateral foot comes off the floor. This is a double support phase since both feet are on the ground. The ankle is generally in neutral position. 30° of hip flexion and 5° knee flexion are achieved [25], [26].

- Loading response: Weight starts to move onto the stance leg when the foot touches the ground, and the knee bends to absorb the impact. The foot swiftly retracts to 10° plantar flexion [25]. The hip gently extends as the knee flexes to 10-15° [27], [28]
- Mid-stance (single-leg support): The body must be able to balance on one leg during midstance while the other leg completes its swing phase. The ankle begins midstance with a slight plantar flexion and, as the heel lifts to begin terminal stance, the ankle gradually dorsiflexes [25]. The hip moves into extension with a steady decrease in flexion, which keeps the trunk upright. At the beginning of midstance, the knee flexes to its maximum, after which the action reverses to extension [27].
- Terminal stance: During this stage, bodyweight shifts to the opposite leg and the heel lifts off the ground. At the end of single-limb support, the ankle is at maximal dorsiflexion (10°), then reverses to achieve 5° of plantar flexion [12]. The hip extends and achieves 10° hyperextension while the knee extends to its maximal range of 0 to -5° [9].
- Pre-swing: In pre-swing the foot leaves the ground, and the limb prepares for swing. Ankle begins to plantarflex quickly before the foot leaves the ground. With the transition from hyperextension to neutral, the hip begins to flex and there is a rapid passive knee flexion [25].

2.1.2 Swing phase

The gait cycle enters swing phase when the foot moves forward without supporting any weight. Leg length may be adjusted throughout the swing phase, and the toes of the swing leg can clear the ground. Swing has three periods [6], [7], [24].

- Toe-off: Toe-off / Initial swing phase starts when the foot is lifted off the ground. This phase includes rapid knee and ankle flexion to enable the swing limb to advance more quickly. At the ankle, dorsiflexion begins [27]. The hip quickly flexes from the neutral position obtained during pre-swing. The 40° position attained during pre-swing is increased by 20° to achieve the 60° knee flexion necessary for toe clearance [27].
- Mid swing: Mid-swing phase occurs when the swing leg approaches the midstance leg

that is supporting body weight. Ankle dorsiflexion to neutral is achieved and then maintained [27]. The leg is raised off the ground by more hip and knee flexion, and as the knee extends the leg swings forward. Hip and knee flexion are 30° at the end of the mid-swing [25].

- Terminal swing: In terminal swing, the knee extends, the foot is brought in front of the body, and the velocity slows. The lower limb gets ready for foot strike and weight shift. The ankle maintains neutral dorsiflexion and may drop into modest plantar flexion (3 to 5°) near the end of this phase [27]. Hips continue to flex at the same 30° angle as mid-swing. The knee keeps extending to its neutral position [25].

2.2 Observational gait analysis

Gait analysis is a systematic study of human movement that involves identifying and measuring the trajectories of various body components across time [29], [30]. Gait analysis is used by clinicians to diagnose gait abnormalities, detect balance factors, assess the success of therapeutic treatments or surgical procedures, and perform necessary therapeutic interventions. Instrumented gait analysis (IGA), the gold standard for gait analysis [3], involves various hardware components such as force plates, reflective markers attached to participants, inertial measurement units, and pressure measurement systems to collect quantitative information (e.g., kinematics, kinetics, muscle activation) and involves analyzing electromyography activity and/or three-dimensional body pose data to diagnose gait abnormalities [4], [31]. Although IGA has been frequently used to examine the gait of children and adults for a variety of clinical applications, this process takes substantial resources; such as, time, money, space, and trained personnel. Motion analysis laboratories are not available in most clinical settings.

To overcome these obstacles, observational gait analysis or visual gait analysis (VGA), an alternative to IGA, provides a procedure for clinicians to observe and describe gait. Visual gait techniques are widely used to evaluate gait issues in children and adults [11], [15], [29], [32]–[34]. In VGA, scorers visually review recorded video and evaluate the recorded gait using a variety of scales that concentrate on specific joints, planes, and events in the gait cycle. Several computer-based image analysis methods have been designed to support clinicians, allowing for joint angle measurement and capturing other motions and postures. Due to its simplicity compared to IGA, this approach is often preferred by clinicians, or the only option available [13]. However, several

authors remarked that VGA is very subjective and may result in low sensitivity, specificity, validity, and reliability when compared to approaches such as IGA. Despite all these potential shortcomings, clinicians still use VGA and depend on it in clinical settings [35].

One of the oldest VGA scoring scales is the Physician Rating Scale (PRS), which was specifically developed for children with CP. Development, reliability, and validity were not well documented when PRS was first published in 1993 [36]. Since then, other VGA scales were proposed that were either designed with a specific patient population in mind or were meant to improve the validity of an existing scale [11], [14], [32], [37]–[44]. Five different gait assessment tools were developed over the last two decades to examine children with CP, with one additional tool focusing on Down Syndrome. For homogeneity, five gait tools specifically designed for CP are included in this review: Physician Rating Scale (PRS), Salford Gait Tool (SF-GT), Observational Gait Analysis (OGA), Observational Gait Scale (OGS), Edinburgh Visual Gait Score (EVGS).

2.2.1 Physician Rating Scale (PRS)

The Physician Rating Scale (PRS) was created by Koman et al. [36] to evaluate sagittal plane gait of children with cerebral palsy. Numerous authors attempted to modify PRS, and several versions are currently available, such as Modified PRS [41], Abbreviated PRS [42], Video Gait Analysis Scoring [43], and Video Gait Assessment Scale [11]. The early PRS was straightforward to use and understand, but lacked sensitivity and reliability in identifying particular changes following therapy [14]. This review discusses the most recent PRS version, Visual Gait Assessment Scale (VGAS), which employed category adjustments following standard three-dimensional gait analysis kinematic data [11]. This scale has seven parameters, four that calculate hip and knee range of motion and three that are foot-specific (heel rise time, initial foot contact, stance foot contact). These parameters are graded on a scale of 1-3 and 1-5, with a total score from 1 to 26 (Figure 2.2).

Parameter	Category Definitions		Score
Hip in terminal stance	Hyperflexed	> 20°	1
	Mod-mild flexion	0° - 20°	2
	Normal (extended)	< 0°	3
Hip in mid swing	Hyperflexed	> 45°	1
	↓ flexion	< 25°	2
	Normal (extended)	25°- 45°	3
Knee peak extension in terminal stance *	Flexion – severe	> 30°	1
	Flexion – mild	16° - 30°	2
	Normal	0° - 15°	3
	Recurvatum	< 0°	4
Knee peak flexion in swing *	Hyperflexed	> 70°	1
	↓ flexion	< 50°	2
	Normal (extended)	50°- 70°	3
Initial foot contact	Forefoot		1
	Foot flat		2
	Heel		3
Foot contact in stance	Toe / toe (equinus)		1
	Foot flat / early heel rise		2
	Foot flat / no early heel rise		3
	Occasional heel / foot flat		4
	Heel / toe (normal roll-over)		5
Timing of heel rise	No heel contact (equinus)		1
	Pre swing / stance limb level		2
	Just after swing / stance limb level		3
	Just pre - double support (normal)		4
	After double support (delayed)		5

* angles also recorded

Figure 2.2 Visual Gait Assessment Scale (VGAS) [11]

Research was conducted to assess inter and intra-observer reliability and validity. The study showed that for experienced observers, modified PRS achieved an acceptable level of inter and intra-observer reliability [37]. For inexperienced observers, PRS was more reliable at the foot and ankle than the hip, which had poor validity. Additionally, PRS was not very accurate in measuring hip motion in the sagittal plane, and specifications of neither transverse nor coronal plane deviations were attempted [37].

2.2.2 Salford Gait Tool (SF-GT)

The Salford Gait Tool (SF-GT) was developed by Toro et al. [12] to evaluate the gait of children with CP. The tool was first designed to evaluate sagittal plane hip, knee, and ankle movement at six gait events: initial contact, end of double support, mid-stance, start of double support, toe-off, and mid-swing. The scores are computed on a five-point scale (-2, -1,0,1,2) with 0 denoting normal

and +/-2 denoting severe abnormality (Figure 2.3). Later, the authors used quantitative kinematic IGA data to modify the upper and lower threshold and overall scores.

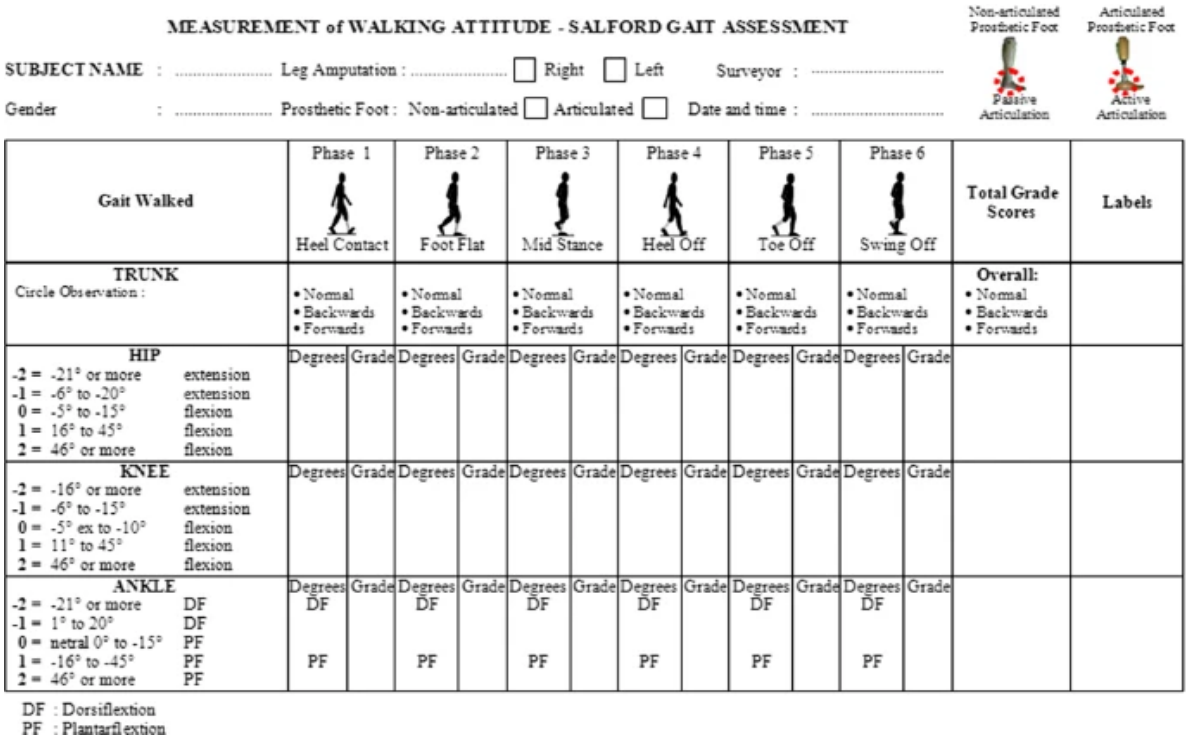

MEASUREMENT of WALKING ATTITUDE - SALFORD GAIT ASSESSMENT

Non-articulated Prosthetic Foot — Passive Articulation

Articulated Prosthetic Foot — Active Articulation

SUBJECT NAME : ..... Leg Amputation : ..... ☐ Right ☐ Left Surveyor : .....

Gender : ..... Prosthetic Foot : Non-articulated ☐ Articulated ☐ Date and time : .....

Gait Walked	Phase 1 Heel Contact		Phase 2 Foot Flat		Phase 3 Mid Stance		Phase 4 Heel Off		Phase 5 Toe Off		Phase 6 Swing Off		Total Grade Scores	Labels
TRUNK Circle Observation :	• Normal • Backwards • Forwards		• Normal • Backwards • Forwards		• Normal • Backwards • Forwards		• Normal • Backwards • Forwards		• Normal • Backwards • Forwards		• Normal • Backwards • Forwards		**Overall:** • Normal • Backwards • Forwards	
HIP -2 = -21° or more extension; -1 = -6° to -20° extension; 0 = -5° to -15° flexion; 1 = 16° to 45° flexion; 2 = 46° or more flexion	Degrees	Grade	Degrees	Grade	Degrees	Grade	Degrees	Grade	Degrees	Grade	Degrees	Grade		
KNEE -2 = -16° or more extension; -1 = -6° to -15° extension; 0 = -5° ex to -10° flexion; 1 = 11° to 45° flexion; 2 = 46° or more flexion	Degrees	Grade	Degrees	Grade	Degrees	Grade	Degrees	Grade	Degrees	Grade	Degrees	Grade		
ANKLE -2 = -21° or more DF; -1 = 1° to 20° DF; 0 = netral 0° to -15° PF; 1 = -16° to -45° PF; 2 = 46° or more PF	Degrees DF / PF	Grade	Degrees DF / PF	Grade	Degrees DF / PF	Grade	Degrees DF / PF	Grade	Degrees DF / PF	Grade	Degrees DF / PF	Grade		

DF : Dorsiflextion
PF : Plantarflextion

Figure 2.3 Salford Gait Assessment [47]

The validity and reliability of this scale were evaluated [37], [38], with a mean agreement of 58% between clinicians and kinematic data based on 5-point scale scoring. The level of agreement between and within observers was high for knee joints but poor for hip joints [45]. Rater experience and clinical experience affect SF-GT inter-rater reliability [46].

2.2.3 Observational Gait Analysis (OGA)

The observational gait analysis (OGA) scale was created by Kawamura et al. [29] for children with CP to compare visual assessment of gait with quantitative gait analysis. OGA is a ten-parameter ordinal scale that assesses the hip, knee, ankle, and pelvis in stance and swing phases and all three planes (sagittal, coronal, transverse). OGA evaluates each parameter as normal, increased, or decreased (Figure 2.4). The final result and research participant kinematic data were compared for analysis.

Sagital Plane

1. Hip at terminal stance:

R	( ) normal extension	( ) decreased extension	( ) increased extension
L	( ) normal extension	( ) decreased extension	( ) increased extension

2. Knee at initial contact:

R	( ) normal flexion	( ) increased flexion	( ) increased extension
L	( ) normal flexion	( ) increased flexion	( ) increased extension

3. Knee at terminal stance:

R	( ) normal extension	( ) increased flexion	( ) hyper extension
L	( ) normal extension	( ) increased flexion	( ) hyper extension

4. Knee at initial swing:

R	( ) normal flexion	( ) decreased flexion	( ) increased flexion
L	( ) normal flexion	( ) decreased flexion	( ) increased flexion

5. Ankle at initial contact:

R	( ) normal dorsiflexion	( ) decreased dorsiflexion	( ) increased dorsiflexion
L	( ) normal dorsiflexion	( ) decreased dorsiflexion	( ) increased dorsiflexion

Coronal plane

6. Pelvic obliquity:

( ) symmetrical ( ) left hemipelvis drop ( ) right hemipelvis drop

7. Hip at loading response:

R	( ) normal adduction	( ) increased adduction	( ) decreased adduction
L	( ) normal adduction	( ) increased adduction	( ) decreased adduction

Transverse plane

8. Pelvic rotation:

( ) symmetrical ( ) right hemipelvis rotated forward ( ) left hemipelvis rotated foward

9. Hip rotation at mid stance:

R	( ) neutral rotation	( ) internal rotation	( ) external rotation
L	( ) neutral rotation	( ) internal rotation	( ) external rotation

10. Foot rotation angle at mid stance (related to the lower limb):

R	( ) neutral rotation	( ) internal rotation	( ) external rotation
L	( ) neutral rotation	( ) internal rotation	( ) external rotation

* Define "Normal" from QGA as all values between 1 Standard Deviation (SD) from the mean, "Increased" as >1SD from the mean and "Decreased" as <1SD from the mean.

Figure 2.4 Observational gait Analysis [31]

Numerous studies were conducted to evaluate OGA validity [14], [22], [33] . Video recordings of children were gathered and analyzed by physical therapists with clinical experience treating CP. Additionally, the observers took a two-month training course on gait analysis and typical gait. Analyses between observers and IGA were evaluated by analyzing manual scores for each video. Finally, statistical analyses were performed to verify the validity of a visual gait analysis compared to kinematic data. Six of the ten variables under analysis had moderate to almost perfect kappa values (i.e., a type of correlation coefficient to assess the inter-rater reliability of qualitative items) between observers. However, only one of these six variables, pelvic obliquity, had high agreement between OGA and IGA [29]. Knee flexion at initial contact and pelvic obliquity had higher inter-

observer agreement and better criterion validity; however, the other eight items were unreliable for visual observation.

2.2.4 Observational Gait Scale (OGS)

The purpose of OGS was to characterize the gait of children with spastic CP [14]. OGS includes 24 parameters: 6 for the foot or ankle, 5 for the knee, 8 for the hip, and the rest for the pelvis. These parameters were chosen with the typical kinematic properties of spastic CP gait in mind. OGS includes observations of joints moving in all three planes [47]. The authors also considered the rater's different levels of training and expertise when developing OGS. The authors further validated OGS criteria and reliability by comparing it to the standard IGA.

2.2.5 Edinburgh Visual Gait Score (EVGS)

The Edinburgh Visual Gait Score (EVGS) was created by Read et al. [15] to evaluate the gait of children with CP. EVGS consists of 17 parameters, each assessed as normal (0), moderate (1), or severe (2). EVGS targets the trunk, pelvis, hip, knee, ankle, and heel in the coronal, sagittal, and transverse planes. Two sets of videos are required to assess these parameters, one capturing gait in the sagittal view and the other in the coronal view.The total score ranges from 0 to 34, where 0 denotes a normal condition and 34 denotes abnormal.

A few studies evaluated the correlation between EVGS and three-dimensional gait analysis [44], [48]–[50]. The average intra-scorer agreement among inexperienced scorers was 5.15, while the mean agreement for experienced scorers was 4.21 [51]. To validate EVGS, 10 numerical parameters from EVGS were compared to three-dimensional gait analysis data. Using Bland and Altman's Coefficient of Repeatability (CoR), inexperienced scorers had total agreement for 52% of the ten numerical parameters and expert scorers had total agreement for 64% (Table 2.1).

Few other researchers attempted to confirm EVGS reliability and validity in gait analysis for experienced observers. However in [52], when compared to three-dimensional gait analysis, inexperienced observers had lower accuracy and experienced observers had higher accuracy. Another study revealed that clinical experience enhanced outcomes [50]. Repeatability might be improved through experience and training based on a comprehensive understanding of gait [53]. Furthermore, EVGS had high concurrent validity due to its substantial agreement with other evaluation techniques and offers an estimate of the gait quality [49], [54].

Table 2.1 Percentage of agreement for EVGS intra-scorer reliability [51]

Parameter	Inexperienced scorers	Experienced scorers
Maximum ankle dorsiflexion in stance (#3)	52	69
Foot rotation (#5)	56	53
Maximum ankle dorsiflexion in swing (#7)	56	83
Peak knee extension in stance (#9)	36	47
Knee extension in terminal swing (#10)	62	55
Peak knee flexion in swing (#11)	29	63
Peak hip extension in stance (#12)	62	75
Peak hip flexion in swing (#13)	58	68
Maximum pelvic obliquity in midstance (#14)	44	55
Pelvic rotation in midstance (#15)	65	69

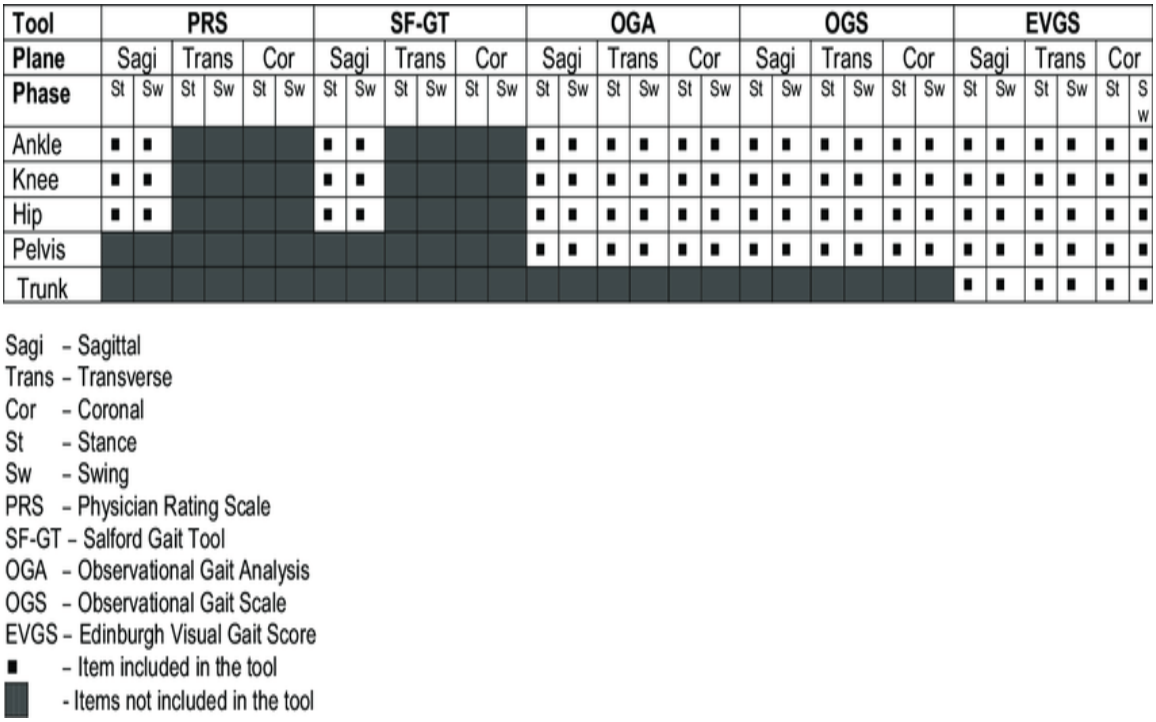

Figure 2.5 Comparison of gait scales [58]

According to a review that analyzed all five gait measures, the PRS is insufficient to capture the entire gait pattern accurately since it has a broad range of variability and only medium reliability and validity findings (Figure 2.5). They argued that OGS should not be used until further study examining its reliability, validity, and clinical application is available. OGS, OGA, or PRS did not contain any references to the original sources. The SF-GT is highly reliable and concurrently valid,

but only assesses sagittal plane gait deviation and requires additional validation [55]. Due to its high reliability and concurrent validity, EVGS is the most effective scale currently available and should be considered when evaluating CP gait patterns [33]. EVGS also includes the trunk, pelvis, hip, knee, and ankle in both the stance and swing phases and data on gait in all three planes.

2.3 Pose estimation

Many clinicians find marker-based motion analysis too expensive and time-consuming, prompting the development of markerless motion analysis systems [56]. Various markerless techniques have been created with differing degrees of accuracy and functionality. Although deep learning-based methods are only one branch of the tree of markerless approaches, deep learning is currently considered the most effective pose estimation method [8], [57], [58].

Top-down and bottom-up approaches are the two primary categories for pose estimation techniques. Top-down techniques begin with person detection and then independently estimate posture inside each bounding box [59]. Detection stage results strongly affect the top-down results. Posture estimation could only produce the anticipated results if the detection method could find the subject of interest [60].

Bottom-up methods first identify the location of body segments or joints before connecting them to each individual [61]. Over the last ten years, several pose estimation algorithms have been published, including Hyperpose [6], OpenPose [5], DeepLabCut [62], Posenet [63], DeepPose [64], Blazepose [7], DeeperCut [65], Alpha-Pose [66]. Using these techniques, it is feasible to use openly accessible pre-trained networks or train new networks tailored to specific research or clinical needs.

2.3.1 Comparison of pose estimation models

DeepPose was based on a regression-based multi-stage human pose estimation technique [64] and was the first approach to use an original deep neural network on human pose estimation. DeepPose demonstrated that a general CNN, created for image classification, could be used for joint localization tasks. The network's performance was compared to results from the then-current state-of-the-art networks using the Frames Labelled In Cinema (FLIC) and Leeds Sports Pose (LSP) datasets, and DeepPose was found to be on par with or outperformed these networks.

A practical approach to identifying 2D poses of many people in a picture was presented by Cao et al. [5] and later made available as the open-source tool OpenPose. The technology first identifies

heat maps of body part locations and part affinity fields that describe how limbs are oriented. The linked limbs for each individual in the image are computed after analysis of the heatmaps and part affinity fields. The proposed approach is highly effective and capable of real-time detecting multiple people's 2D poses.

Table 2.2 Pose estimation model keypoints

	DeepPose	**HyperPose**	**BlazePose**	**OpenPose**
Skeleton Model		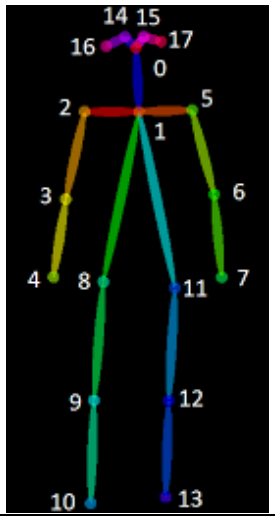	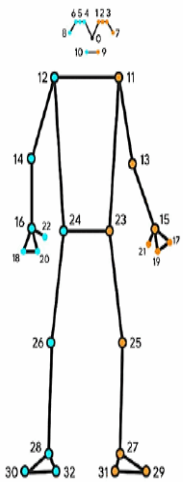	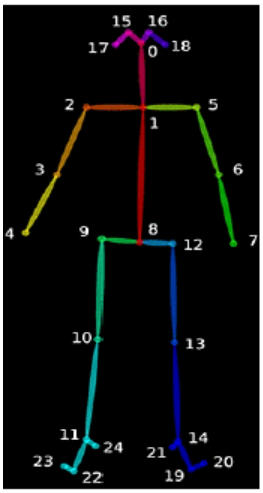
Reference	[64]	[6], [67]	[7], [68]	[5], [67]–[69]
Neck / trunk start	Yes	Yes	No	Yes
Mid hip / trunk ending	No	No	No	Yes
Hip	Yes	Yes	Yes	Yes
Knee	Yes	Yes	Yes	Yes
Ankle	Yes	Yes	Yes	Yes
Heel	No	No	Yes	Yes
Toes	No	No	Yes	Yes

However, AI models like OpenPose may need substantial processing, making implementation difficult. Another model, HyperPose, uses a less computationally intensive variant of OpenPose while optimizing several GPU operations. By combining NVIDIA's Compute Unified Device

Architecture (CUDA) architecture and TensorRT deep learning optimization package, HyperPose offers an optimum method of executing inferences [6]. Another smartphone-friendly model, BlazePose [7], has a two-step detector-tracker inference pipeline. The tracker follows the person in consecutive frames once the detector has finished running on the initial frame or until a person is found.

In research comparing OpenPose and HyperPose performance [67], OpenPose BODY25 consistently classified body keypoints more accurately than HyperPose. Other studies that contrasted OpenPose and BlazePose showed that the OpenPose performed better than BlazePose when predicting human pose estimation coordinates [68]. However, there was a trade-off between algorithm accurate keypoint detection and speed. OpenPose was recommended for pose estimation that required more accurate keypoint identification [45] [46]. As shown in Table 2.2, when compared to other widely used pose estimation methods, OpenPose provides all the necessary inputs to compute EVGS.

2.3.2 OpenPose – real-time 2D pose estimation

OpenPose can provide real-time, open source, 2D human pose estimation technique. This is a bottom-up method for estimating poses. Part Affinity Fields (PAFs) are used to identify a person's body parts in pictures or videos. Figure 2.6 shows the overall pipeline.

OpenPose architecture

1. The system receives a color image, then analyzes the image using a CNN that was initialized and tweaked using the top 10 VGG-19 layers (Trained Convolutional Neural Network).
2. A second multi-stage CNN is given a collection of feature maps created by the first CNN.
3. The initial set of stages predicts and improves PAFs, a collection of 2D vector fields representing the strength of the link between body parts.
4. The final set of steps creates confidence maps of the body part locations
5. To get 2D keypoints for each individual in the picture, the confidence maps and PAFs are processed using bipartite matching.

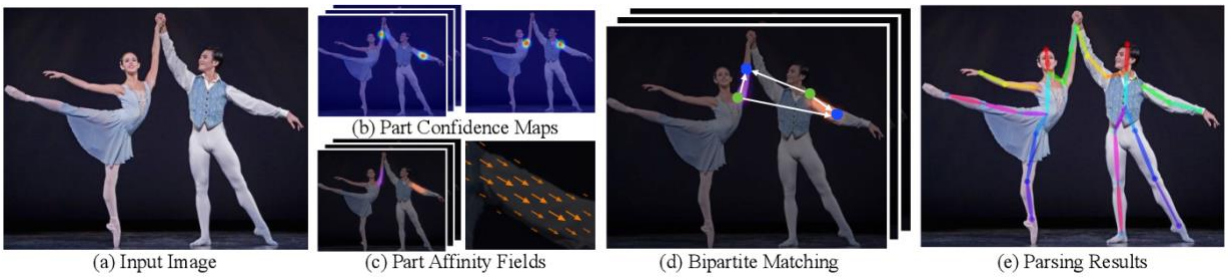

Figure 2.6 OpenPose overall pipeline [5]

Part affinity fields for part association

PAFs include position and orientation data for the area where the limb is supported. A series of flow fields encode the link between bodily parts in an unstructured pairwise manner. There is one PAF for every pair of bodily components. PAFs are represented as the set L = (L_1, L_2, ..., L_c), where $L_c \in \mathbb{R}^{w*h*2}, c \in \{1 .. C\}$. The input image's size is $w * h$, and C represents the number of pairs of body parts. Every image location in the L_c encodes a 2D vector; if the location is on the limb c that connects the body parts j_1 and j_2, the value of the PAF at that position is a unit vector pointing from j_1 to j_2; otherwise, the vector has a zero value. The ground truth PAF $L^*_{c,k}$ at point p for person k is described by equation (2.1).

$$L^*_{c,k}(p) = \begin{cases} \dfrac{X_{j_2,k} - X_{j_1,k}}{\| X_{j_2,k} - X_{j_1,k} \|_2} & \text{if p is on limb} \\ 0 & \text{otherwise} \end{cases} \tag{2.1}$$

Confidence maps for part detection

Each confidence map is a 2D representation that reflects the belief or probability that a specific body part is located within a particular pixel of an image. One confidence map corresponds to each body component. Confidence maps are the set $S = S_1, S_2, \dots, S_j$, where $S_j \in \mathbb{R}^{w*h}, j \in \{1 \dots J\}$, and J specifies the number of body parts. Equation (2.2) provides individual confidence maps for each person k, where $x_{j,k}$ represents the location of body component j on person k. A collection of distinct confidence maps given in equation (2.3) makes up the ground truth confidence map

$$S^*_{j,k}(p) = \exp\left(-\frac{\|p - x_{j,k}\|_2^2}{\sigma^2}\right) \tag{2.2}$$

$$S_j^*(p) = \max_k S_{j,k}^*(p) \tag{2.3}$$

Multi-structures in OpenPose

OpenPose models (Figure 2.7) employ a multi-structured approach in which two different CNNs are combined at each stage. For each desired keypoint, network one predicts a confidence map and network two predicts an affinity field outlining the strength of the relationship between various keypoints.

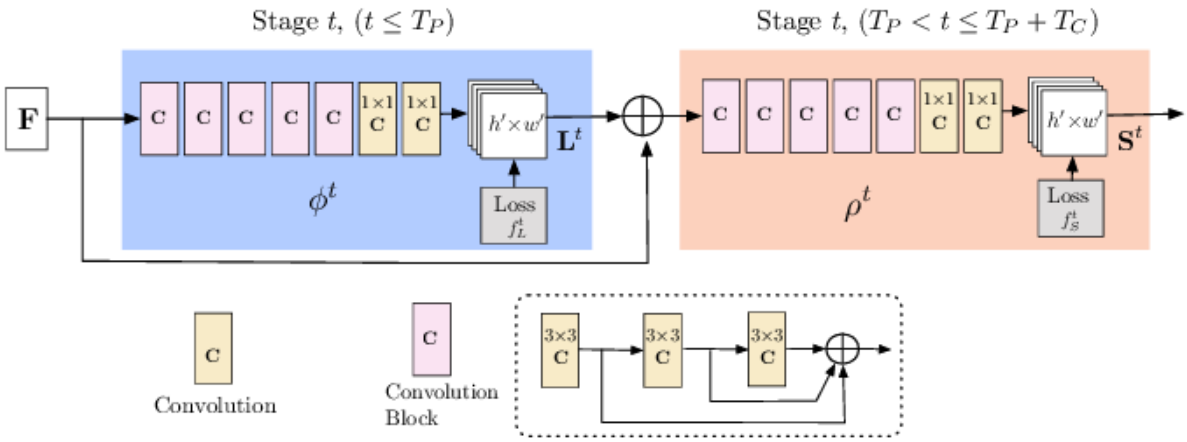

Figure 2.7 Multi-structured architecture used in OpenPose [73]

2.4 Automated Gait Analysis

In the field of automated gait analysis, various approaches have been developed to capture and analyze human movement during walking. Reference [70], addressed markerless gait analysis in three stages: image preprocessing, gait figure extraction, and motion analysis based on joint angles. The image sequences used in this study were recorded at a normal walking speed, with subjects filmed from different angles while walking on a treadmill. Although this research explored automatic gait analysis, their approach did not utilize handheld videos or scoring scales. Abi Hayla Myriam, et al. [71] developed software for automated gait analysis based on the Rancho Observational Gait Analysis approach, identifying gait deviations and their causes. However, their software was not tested and some issues needed to be resolved, including automatic reporting and synchronization with Visual 3D analysis software. Adithya et al. [72] proposed a marker-less, cost-

effective, and user-friendly approach utilizing a mobile phone camera and 2D pose estimation system to capture important anatomical landmarks. They only calculated knee flexion/extension angle.

2.5 Conclusion

IGA is often used to assess children, but this approach requires time, specialized equipment, space, and skilled personnel. Visual gait analysis (VGA), an alternative to IGA, has become popular with physicians and is used in clinical settings due to several benefits; specialized equipment is not required, VGA can be performed in practically any setting, and this approach is more affordable than IGA. EVGS is a preferred scale among the many visual gait scales because of its high concurrent validity and reliability [55]. To date, EVGS scoring methods are not automated; instead, they depend on a person to review videos, pause videos at precise gait events, and analyze gait; a time-consuming process for clinical applications. With improvements in AI pose inference models, AI algorithms could be used to generate automated EVGS scores for clinical application and long-term care.

3 Edinburgh Visual Gait Score

This chapter introduces and explains the Edinburgh Visual Gait Scale (EVGS) analysis.

The Edinburgh Visual Gait Score (EVGS) has 17 parameters for each lower extremity, for a total of 34 parameters. Five of the 17 parameters are within swing phase, with the rest in stance. The seventeen EVGS parameters are: initial contact, heel lift, maximum ankle dorsiflexion in stance, foot clearance in swing, maximum ankle dorsiflexion in swing, peak knee extension in stance, knee position in terminal swing, peak knee flexion in swing, peak hip extension in stance, peak hip flexion in swing, pelvic rotation at midstance, peak sagittal trunk position in stance, hindfoot varus/valgus in stance, knee progression angle at midstance, foot rotation in stance, pelvic obliquity at midstance, maximum trunk lateral shift.

In practice, a person's gait in sagittal and coronal views are video recorded while walking, using a handheld camera or a camera on a tripod. Typical clinical practice is that the video is scored by a human according to the EVGS guidelines. The person scoring the video can use video editing software to pause the recorded video at specific gait events for analysis. Software can also be used to determine joint angles and other EVGS parameters.

A 3-point ordinal scale is used to score each parameter. 0 = normal (within +/- 1.5 standard deviations of the mean), 1 = moderate deviations (between 1.5 and 4.5 standard deviations of the mean), 2 = significant/severe deviations (more than 4.5 SD of mean). Multiple strides can be scored for each parameter, and the most common score across all strides is retained. After scoring all parameters for each leg, the scores for each leg are summed (highest total score = 34). A lower overall score indicates less gait deviation [15].

To enhance understanding and maintain consistency, the 17 EVGS parameters are grouped based on foot events and gait cycle phases. For the sagittal view, parameters are categorized into initial contact/terminal swing, midstance, terminal stance, and midswing. Meanwhile, for the coronal view, parameters are grouped into midstance. Table 3.1 below lists the parameters and how they are organized according to these events.

Table 3.1 List of EVGS parameters

	Foot events and gait phases	EVGS parameters
Sagittal view	Initial contact/Terminal swing	Peak hip flexion in swing(#13)
		Knee extension in terminal swing (#10)
		Initial contact (#1)
	Midstance	Peak sagittal trunk position (#16)
		Pelvic rotation in midstance (#15)
		Heel lift (#2)
	Terminal stance	Peak hip extension in stance (#12)
		Peak knee extension in stance (#9)
		Max ankle dorsiflexion in stance (#3)
	Midswing	Peak knee flexion in swing (#11)
		Maximum ankle dorsiflexion in swing (#7)
		Foot clearance in swing (#6)
Coronal view	Midstance	Maximum lateral shift of trunk (#17)
		Maximum pelvic obliquity in stance (#14)
		Knee progression angle (#8)
		Foot rotation (#5)
		Hindfoot valgus/varus (#4)

In the following subsections, each of the parameters will be introduced and discussed in turn.

3.1 Sagittal view parameters

The EVGS parameters can be grouped by gait period: initial contact, mid stance, terminal stance, mid swing.

3.1.1 Initial contact/ Terminal swing

Peak hip flexion in swing (#13)

The hip anatomy allows for a wide range of motion in three axes: transverse, longitudinal, and sagittal. The transverse axis provides flexion and extension movements. Hip flexion is leg movement toward the front and extension is leg movement toward the back. Normal hip flexion ranges from 25° to 45° [15]. Figure 3.1 shows right leg hip flexion and hip extension.

(a) **(b)**

Figure 3.1 Right leg hip flexion (a) and extension (b)

Knee extension in terminal swing (#10)

Knee flexion involves reducing the angle between the thigh and the shin, as in curling the heel toward the gluteal muscles. Knee extension refers to rotating the shank forward, such as when kicking the leg straight. Figure 3.2 shows right knee flexion and extension.

Initial contact (#1)

Typically, "heel contact" with the floor occurs first in the gait cycle (Figure 3.3 (a)). “Toe contact” occurs when the toe-part of the foot distal to the metatarsophalangeal joints makes initial contact with the ground (Figure 3.3 (b)). "Flatfoot contact" occurs when the heel and toe make simultaneous contact (Figure 3.3 (c)).

(a) (b)

Figure 3.2 Right leg knee flexion (a) and extension (b)

(a) **(b)** **(c)**

Figure 3.3 (a) Heel contact, (b) toe contact, (c) flatfoot contact

Table 3.2 lists the sagittal parameters that must be examined in the initial contact period.

Table 3.2 Sagittal view - initial contact parameters

EVGS Parameter	Criteria	Score
Peak hip Flexion in Swing(#13)	Marked increase (> 60° flexion)	2
	Increased (46° - 60° flexion)	1
	Normal (25°–45° flexion)	0
	Reduced (10° - 24° flexion)	1
	Severely reduced (< 10° flexion)	2
Knee extension in terminal swing (#10)	Severe (> 30° flexion)	2
	Moderate (16° - 30° flexion)	1
	Normal (5°–15° flexion)	0
	Moderate overextension (4° flexion - 24° extension)	1
	Severely hyperextension (> 10° extension)	2
Initial contact (#1)	Heel contact	0
	Flatfoot contact	1
	Toe contact	2

3.1.2 Midstance

Peak sagittal trunk position (#16)

Although the trunk will not move through a wide range of motion in the sagittal plane, its posture and movement can still affect lower extremity gait patterns. The trunk usually maintains an upright position during the stance and swing phases. A normal range of motion is less than 5° backward or forward. The moderate range is defined as 6° to 15° forward (Figure 3.4 (a)) or more than 5° backward (Figure 3.4 (b)), while the severe range is more than 15° forward (Figure 3.4 (c)) [15].

Pelvic rotation in midstance (#15)

During midstance the pelvis moves forward on the swing side, whereas the pelvis rotates backward on the stance side. The pelvis should be neutrally rotated in midstance, between 5° retraction of the stance leg and 0° forward rotation. More forward and backward rotation is required for a moderate to severe condition [15].

(a) **(b)** **(c)**

Figure 3.4 (a) Moderate, (b) reduced, (c) marked peak sagittal position of trunk

Heel lift (#2)

Heel lift typically occurs between midstance and terminal stance or between the opposing swing foot being level with the stance foot and the swing foot making contact with the ground. "Early" heel lift" occurs when stance foot heel lift occurs before the swing foot is level with the stance foot or before midstance (Figure 3.5 (a)). "Delayed heel lift" is when heel off occurs after terminal stance, that is before or after opposite foot contact (Figure 3.5 (b)). "No heel contact" refers to the absence of contact between the heel of the foot and the ground during the stance phase. "No forefoot contact", an infrequent calcaneus foot condition, occurs when the forefoot does not touch the ground during stance [15]. Table 3.3 lists the sagittal parameters that must be examined in the gait event's midstance position.

(a) **(b)**

Figure 3.5 (a) Early heel lift, (b) Delayed heel lift.

Table 3.3 Sagittal view – midstance parameters

EVGS Parameter	Criteria	Score
Peak sagittal trunk position (#16)	Marked forward (>15° forward)	2
	Moderate forward (6° - 15° forward)	1
	Normal upright (vertical to 5° back or forward)	0
	Moderate backward (> 5° back)	1
Pelvic rotation in midstance (#15)	Marked retraction (> 15°)	2
	Moderate retraction (6° - 15°)	1
	Normal (5° retraction - 10° protraction)	0
	Moderate protraction (11° - 20°)	1
	Severe protraction (> 20°)	2
Heel lift (#2)	No forefoot contact	2
	Delayed	1
	Normal	0
	Early	1
	No heel contact	2

3.1.3 Terminal stance

Peak hip extension in stance (#12)

Normal hip extension in stance ranges from neutral to 20° [15].

Peak knee extension in stance (#9)

In a terminal stance, the knee almost entirely extends. A knee remaining more flexed throughout stance is abnormal gait [15]. As the femur advances over a tibia that has been halted, hyperextension may develop.

Maximum ankle dorsiflexion in stance (#3)

The normal ankle dorsiflexion range occurs when the tibia moves forward across the hindfoot at first contact to dorsiflexion at the end of the stance while keeping the heel in touch with the ground. Therefore, regardless of where the foot is positioned on the floor, the tibia-hindfoot angle is recorded for this parameter. Excessive plantarflexion or excessive knee flexion can contribute to abnormal gait and prevent the heel from making contact [15]. Figure 3.6 shows ankle dorsiflexion and plantarflexion. Table 3.4 lists the sagittal parameters that must be examined in the gait event's terminal stance position.

(a) **(b)**

Figure 3.6 (a) Dorsiflexion, (b) plantarflexion

Table 3.4 Sagittal view – terminal stance parameters

EVGS Parameter	Criteria	Score
Peak hip extension in stance (#12)	Severe (> 15° flexion)	2
	Moderate (1° - 15° flexion)	1
	Normal (0°–20° extension)	0
	Moderate hyperextension (21°- 35° extension)	1
	Severely hyperextension (> 35° extension)	2
Peak knee extension in stance (#9)	Severe (> 25° flexion)	2
	Moderate (16° - 25° flexion)	1
	Normal (0°–15° flexion)	0
	Moderate hyperextension 1° - 10° extension)	1
	Severely hyperextension (> 10° extension)	2
Max ankle dorsiflexion in stance (#3)	Excessive dorsiflexion (> 40°)	2
	Increased dorsiflexion (26° - 40°)	1
	Normal (5°–25° dorsiflexion)	0
	Reduced dorsiflexion (10°plantarflexion - 4°)	1
	Marked plantarflexion (> 10°)	2

3.1.4 Mid swing

Peak knee flexion in swing (#11)

Knee flexion in swing phase is required to lift the lower extremity off the ground to proceed into initial contact, and the toe will touch the ground if there is insufficient knee flexion. Knee flexion is usually between 50° and 70° [15].

Maximum ankle dorsiflexion in swing (#7)

During swing phase, the ankle should be neutral to slightly plantarflexed (5°) [15].

Foot clearance in swing (#6)

The foot should be completely off the ground during the swing phase, referred to as "full clearance". Extreme lifting of the foot above the ground is referred to as "high steps." Reduced clearance is when the foot is barely lifted off the ground during swing phase. "None" denotes no foot off throughout swing phase, where part of the foot is always in contact with the ground [15].

Table 3.5 lists the sagittal parameters that must be examined in midswing.

Table 3.5 Sagittal view – midswing parameters

EVGS Parameter	Criteria	Score
Peak knee flexion in swing (#11)	Severely increased (> 85° flexion)	2
	Moderately increased (71° - 85° flexion)	1
	Normal (50°–70° extension)	0
	Moderately reduced (35° - 49° flexion)	1
	Severely reduced (< 35° flexion)	2
Maximum ankle dorsiflexion in swing (#7)	Excessive dorsiflexion (> 30°)	2
	Increased dorsiflexion (16° - 30°)	1
	Normal (15° dorsiflexion - 5° plantarflexion)	0
	Reduced plantarflexion (6° - 20° plantarflexion)	1
	Marked plantarflexion (> 20° plantarflexion)	2
Foot clearance in swing (#6)	High steps	1
	Full clearance	0
	Reduced clearance	1
	None	2

3.2 Coronal view parameters

3.2.1 Midstance

Maximum lateral shift of trunk (#17)

During stance phase, the trunk moves 25 mm side to side towards the weight-bearing leg, which is considered "normal." More than 25 mm of lateral flexion can be considered moderate to marked lateral trunk shift (Figure 3.7). When the trunk stays bending over the opposite side, that is swinging leg, trunk shift is "reduced" (Figure 3.7 (c)) [73].

Maximum pelvic obliquity in midstance (#14)

During stance, the pelvis usually drops slightly to the other side before leveling at terminal stance. To determine whether the pelvis is "Up" (Figure 3.8 (a)) or "Down," (Figure 3.8 (b)) the anterior superior iliac spine (ASIS) should be evaluated in midstance in relation to the ASIS on the other side [15].

(a) **(b)** **(c)**

Figure 3.7 (a) Moderate and (b) severe lateral trunk shift on right leg. (c) Reduced trunk shift on left leg

(a) **(b)**

Figure 3.8 (a) Up and (b) down pelvic obliquity on right leg

Knee progression angle (#8)

The knee progression angle (KPA) is the direction the patella points with respect to the walking path. During the gait cycle, the knee often points forward, which is considered "normal." A score of 1 is for an internal or external rotated knee with the complete kneecap visible, and a score of 2 is for a rotated knee with only the part of the knee visible [15]. Figure 3.9 shows the externally rotated knee with the knee cap fully and partially visible and the internally rotated knee with the knee cap fully and partially visible.

(a) **(b)** **(c)** **(d)**

Figure 3.9 Right leg externally rotated (a) entire kneecap visible, (b) part kneecap visible. Right leg internally rotated (c) entire kneecap visible, (d) part kneecap visible

Foot rotation (#5)

The foot progression angle is "normal" when the foot is somewhat externally rotated in relation to KPA [15]. Figure 3.10 shows internal and external foot rotation.

(a) **(b)**

Figure 3.10 Right foot (a) externally rotated (b) internally rotated

Hindfoot valgus/varus (#4)

Valgus is when the mid-calcaneal axis, the line that imaginarily connects the center of hindfoot with the middle toe, deviates from the body's midline, also known as eversion or pronation. Varus, also known as inversion or supination, occurs when the mid-calcaneal axis moves toward the body's midline (Figure 3.11). The hind foot is in "normal" condition when it is neutral or mildly valgus. Table 3.6 lists the coronal parameters that must be examined in midstance.

(a) **(b)**

Figure 3.11 (a) Hindfoot varus, (b) hindfoot valgus

Table 3.6 Coronal view – midstance parameters

EVGS Parameter	Criteria	Score
Maximum lateral shift of trunk (#17)	Severe lateral trunk shift	2
	Moderate increased lateral shift	1
	Normal (approx. 25 mm over stance leg)	0
	Reduced lateral shift of trunk	1
Maximum pelvic obliquity in stance (#14)	Marked down (> 10°)	2
	Moderate down(1° - 10°)	1
	Normal (0 - 5° up)	0
	Moderate up (6° - 15°)	1
	Marked up (> 15°)	2
Knee progression angle (#8)	External, part knee cap visible	2
	External, all knee cap visible	1
	Neutral, knee cap midline	0
	Internal, all knee cap visible	1
	Internal, part knee cap visible	2
Foot rotation (#5)	Marked external >KPA (by >40°)	2
	Mod external >KPA (by 21°–40°)	1
	SI more external than KPA (by 0°–20°)	0
	Mod internal >KPA (by 1°–25°)	1
	Marked internal >KPA (by >25°)	2
Hindfoot valgus/varus (#4)	Severe valgus (> 15°)	2
	Moderate valgus (6° - 15°)	1
	Neutral/slight valgus (0° - 5° valgus)	0
	Mild varus (1° - 10°)	1
	Severe varus (> 10°)	2

4 Algorithm Development

This chapter discusses the development of an algorithm for calculating EVGS.

To achieve the automated EVGS analysis objective, the proposed system must be able to identify the appropriate video frames for analysis and then apply a series of rules to generate scores for each parameter. This involves two main tasks: creating a method for identifying the required gait events in a walking video and creating an algorithm for scoring the EVGS parameters.

This chapter outlines the techniques and procedures used to implement stride detection and compute the automatic EVGS score. Figure 4.1 provides the flowchart outlining the proposed methodology for automatically scoring EVGS. The proposed methodology is to sequentially implement pose estimation, view detection, direction of motion detection, gait event identification, stride allocation, and finally algorithmic scoring of the EVGS. The details of each step are provided in different sections. Section 4.1 presents the pose estimation step. Section 4.2 combines view detection, direction of motion detection, gait event identification, and stride allocation into gait event and stride detection. Section 4.3 presents the algorithmic implementation of EVGS.

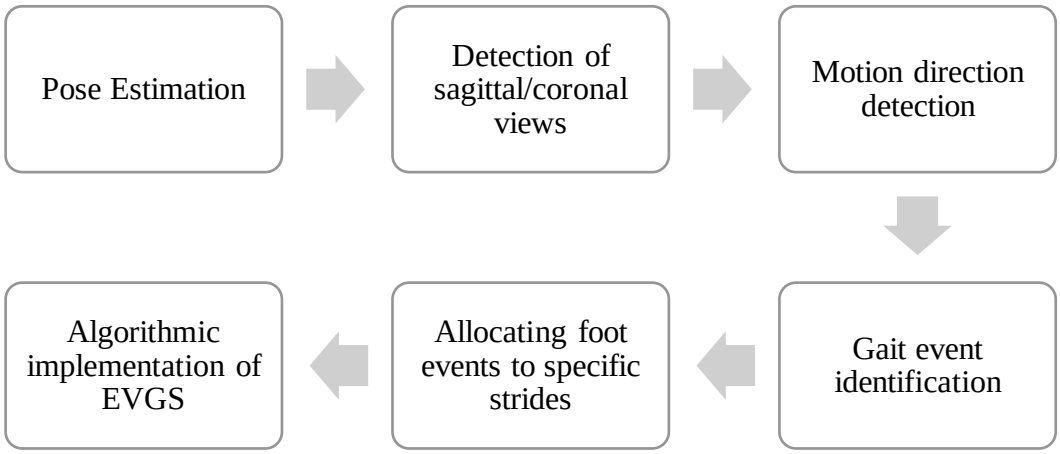

Figure 4.1 Overall methodology for calculating EVGS

A preliminary set of videos is needed to develop the algorithm. To obtain these videos, an able-bodied individual walking in both sagittal and coronal views was recorded using a 60hz handheld smartphone camera. The researcher manually labeled the ground truth of foot events in these videos and evaluated each EVGS parameter, assigning scores accordingly. The algorithm for stride

detection and EVGS evaluation was developed using this manually labeled ground truth of foot events and the corresponding manual EVGS scores

4.1 Pose estimation

For each video frame, the OpenPose-BODY25 model provided joint coordinates as keypoints (Figure 4.2). Trajectories along the x and y coordinates can be noisy and sometimes contain outliers, which indicates that the tool could not detect the proper position of that particular keypoint. 2D keypoint data includes confidence scores that indicate the likelihood that the keypoints were placed correctly.

Video keypoint data were filtered using a zero-phase second-order low-pass Butterworth filter with a cut-off frequency of 12 Hz. The Butterworth filter provides the ideal trade-off between phase responsiveness and attenuation. Because Butterworth filters have the sharpest roll-off attainable for a given order without producing peaking in the Bode plot, they are known as maximally flat filters. The Butterworth filter is a good option for organizing the multiple poles of higher-order filters used in control systems [74]. To avoid Butterworth filter phase shift, the signal was processed both forwards and backwards (i.e., dual pass).

Figure 4.2 OpenPose algorithm output example

The 2D keypoint processing strategy was adapted from earlier work done for a marker-less AI motion-analysis method for hallways [75]. Video keypoint data were improved by removing

keypoints with scores below a 10% threshold. After that, cubic spline interpolation was used to fill gaps of five frames (0.083 s) or fewer.

4.2 Gait event and stride detection

Gait event identification was the next and most crucial stage of this project. Foot strike and foot off are specific events in the gait cycle, while midstance and midswing are periods of the gait cycle that occur over a number of frames. To determine the EVGS accurately, the specific frame number where the peak of the period occurs must be identified. The midpoint of midstance and midswing were labelled as mid-midstance and mid-midswing. Initial contact, mid-midstance, toe off, and mid-midswing must be identified for the EVGS score. The process involved determining if the video is in the sagittal or coronal plane; determining whether the motion is going left to right, right to left, anterior to posterior, or posterior to anterior; detecting the four distinct gait events; and assigning values to a particular stride.

4.2.1 Detection of sagittal/coronal views

An algorithm was developed to track the distance between the top chest and mid-hip keypoints (trunk length). The algorithm considers a video to be sagittal when the absolute difference between the distances in the first and last frames is less than a threshold (99 pixels). To identify the threshold, 37 videos of able-bodied people walking in both coronal and sagittal views were analyzed. A difference in trunk length of less than 99 pixels produced the best results, where the video resolution was 1920 x 1080. Therefore, 99 pixels was set as the cutoff point for classifying sagittal plane walking.

In the front view, when the person is far away from the camera, the keypoints appear in a small area and as the person moves closer to the camera the keypoint coordinates reach their maximum values, causing the trunk length to reach its maximum when the person is close to the camera (Figure 4.3 (a)). Trunk length reduces from maximum when the person walks away from the camera (Figure 4.3 (b)). Trunk length fluctuates very little when walking in the sagittal plane, and trunk length stays within the threshold (Figure 4.4).

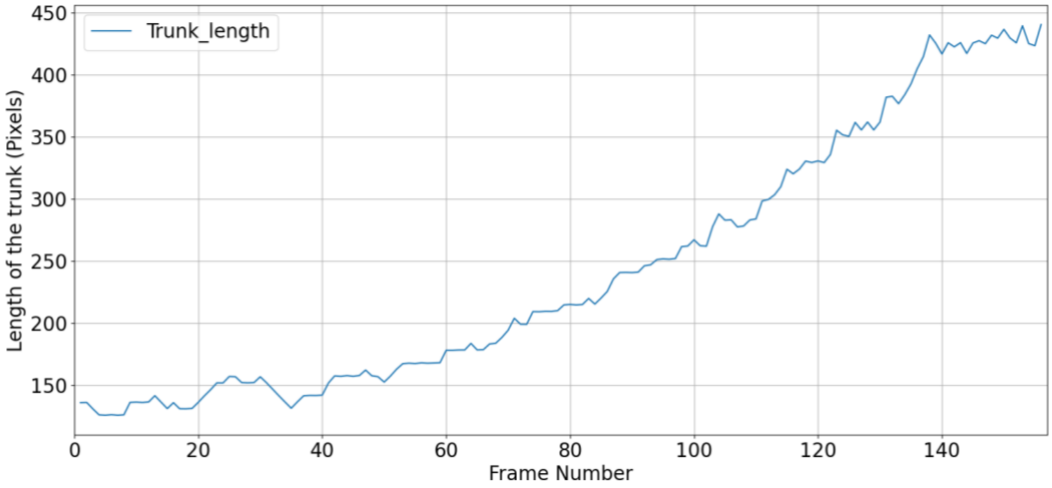

(a)

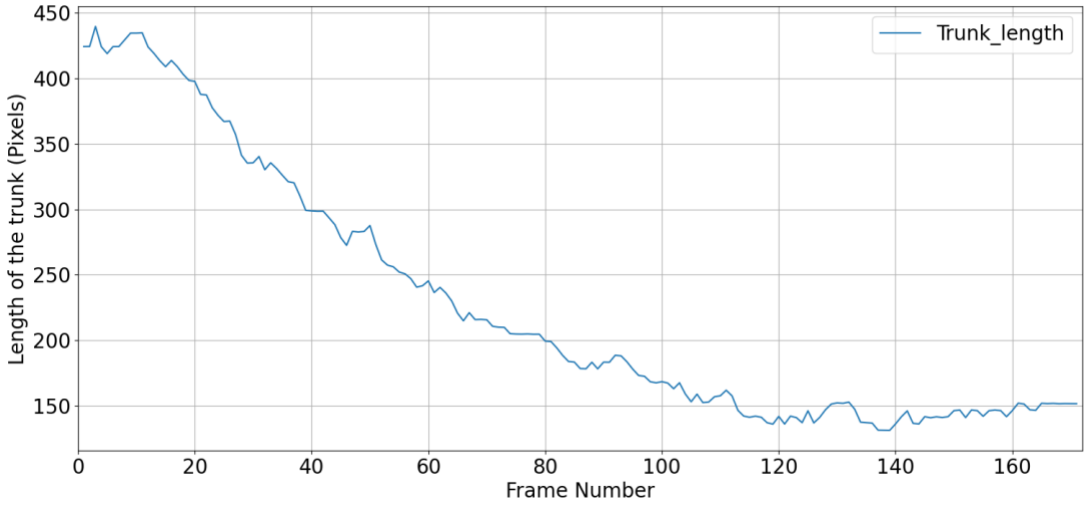

(b)

Figure 4.3 Trunk length in coronal view. Participants moved (a) toward camera, (b) away from the camera.

4.2.1 Motion direction detection

Following the coronal or sagittal identification of the video, the next step would be to determine frontal or rear in coronal view and left to right or right to left in sagittal view.

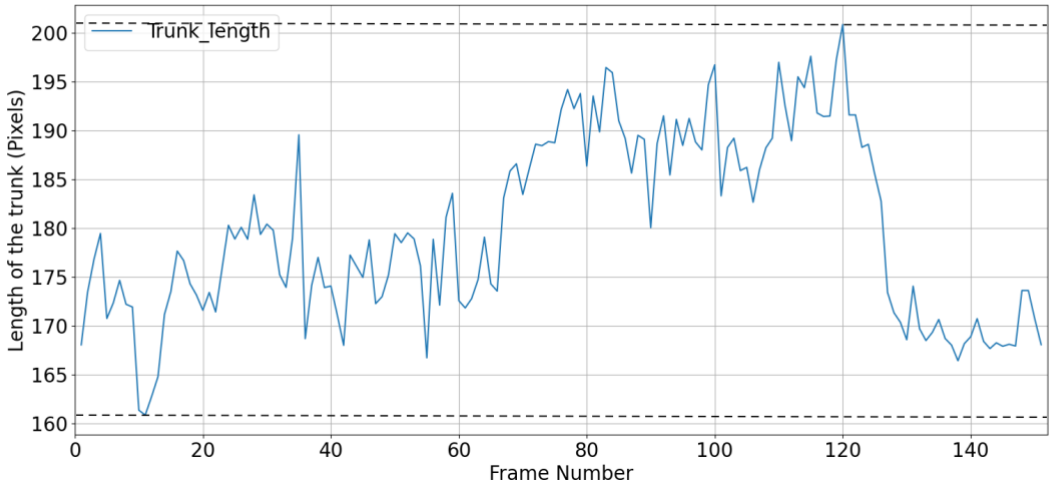

Figure 4.4 Trunk length in sagittal view. Black dashed lines shows that the change in trunk length remained within the 99-pixel threshold

Coronal view

After categorizing the video as coronal, the algorithm determines the person's walking direction in the coronal plane (frontal or rear). Two techniques were applied, the point where the shoulder and hip keypoints intersect and the trunk length.

In the first method, the algorithm attempted to recognize turns in videos that included a person walking in both frontal and rear views. Turns were detected by identifying the optimal crossing point between the shoulder and hip keypoints. The turning point was determined by tracking the shoulder and hip along the x-axis. The ground truth was labelled and compared to the identified turning point. This approach detected turns a few frames in advance (Figure 4.5), which was not appropriate for accurately identifying motion direction. Hence, a second method was employed in which the algorithm replicated the approach for locating the sagittal/coronal views. The algorithm monitors the trunk length and compares the difference between the first and final frames. If the difference is negative, the participant is facing forward and if the difference is positive, the person is going away from the camera.

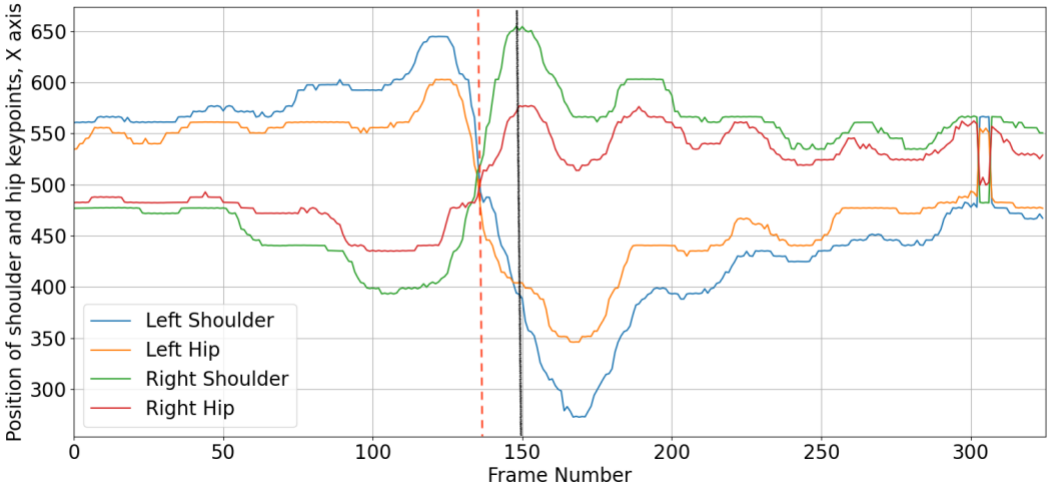

Figure 4.5 Turning point selection based on hip and shoulder keypoints. The solid line represents the detected frame, whereas the dashed line represents the ground truth.

Sagittal view

In the sagittal view, the algorithm tracks the nose location on the x-axis and calculates the difference between nose positions in the first and final frames. X-coordinates are maximal at the right border and minimal at the left border. Using this concept, if the difference is negative, the person is walking from left to right (Figure 4.6). If the difference is positive, the person walks from right to left .This method produced consistent results.

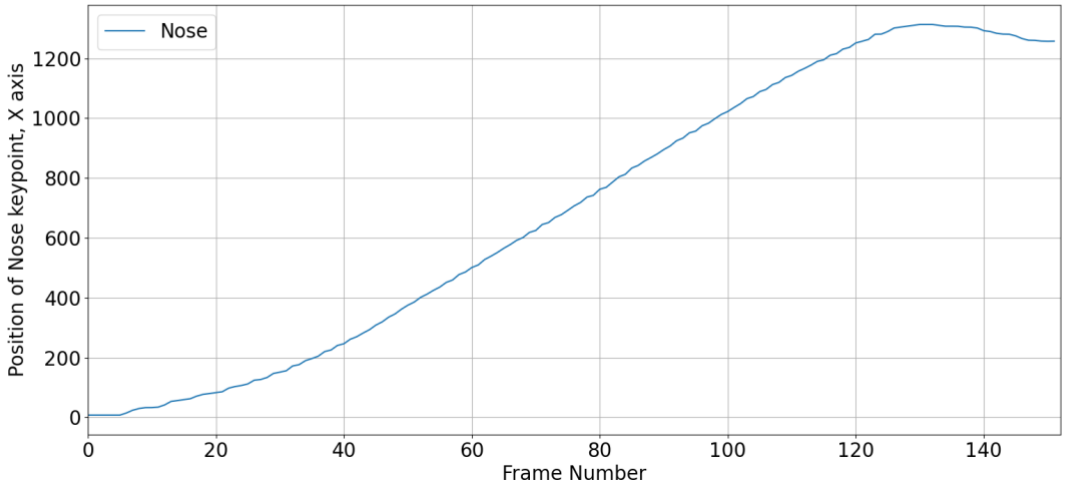

Figure 4.6 Left to right direction detection based on nose keypoint.

4.2.2 Gait event identification

Sagittal view

Initial contact was determined by foot strike and terminal stance by foot off. The Zeni et al. [76] method was employed to identifying foot strike and foot off. According to this approach, heel-strike is when the sacral marker forward distance from the heel marker is at its maximum and toe-off is when the toe marker is furthest posterior from the sacral marker. Since sacrum keypoints are not provided in OpenPose, the midhip keypoint was used to replace the sacral marker location. Figure 4.7 provides an example of identified foot strikes and foot off using the heel position and mid-hip positions.

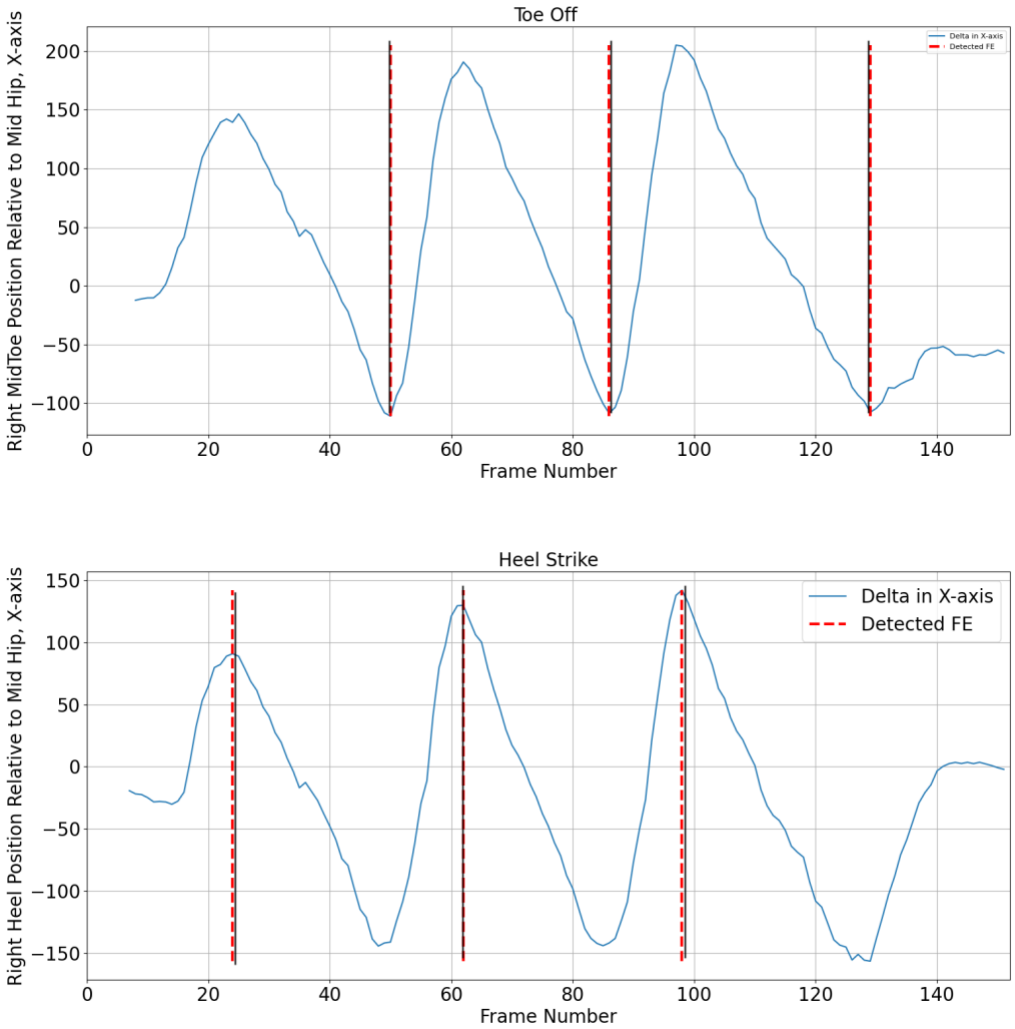

Figure 4.7 Identification of heel strike and toe off for right leg (top) mid-toe position, (bottom) heel position. Solid black line represents actual foot event frame and dashed red line is estimated foot event.

The distance between the knees is measured to determine mid-midstance and mid-midswing. The legs are closer together in mid-midstance posture; hence, the distance between the two knees would be less at that time. Assuming that the right knee is (x_1, y_1) and the left knee is (x_2, y_2), the distance between knees was calculated using equation 4.1 and mid-midstance was at the minimum distance.

$$d = \sqrt{(x_2 - x_1)^2 + (y_2 - y_1)^2} \tag{4.1}$$

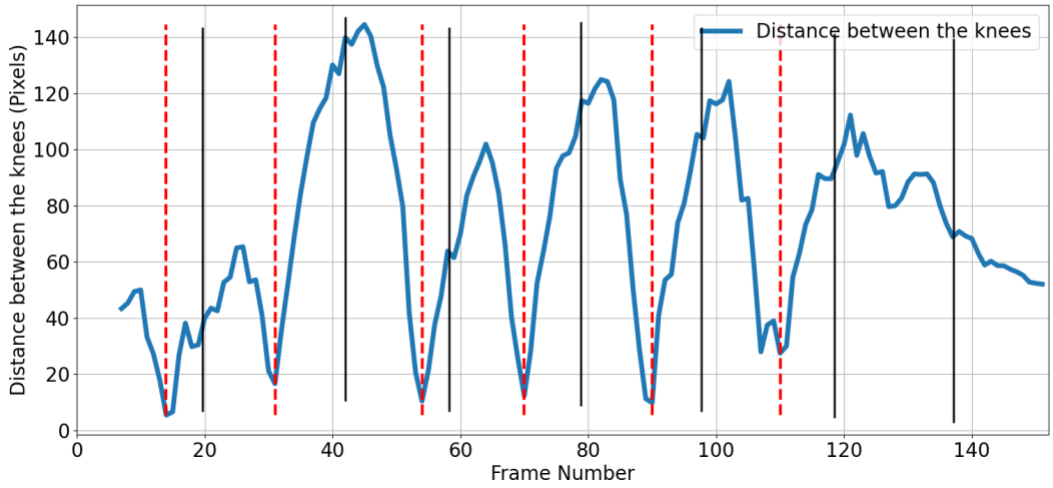

Figure 4.8 Mid-midstance detection using knee distance. Dashed red line shows algorithmically calculated mid-midstance. Solid black line shows actual frame number of the mid-midstance.

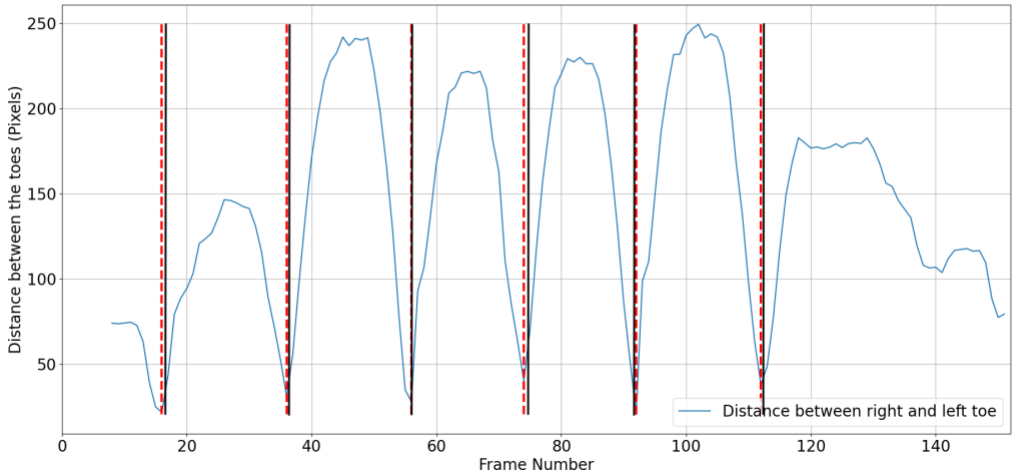

Figure 4.9 Mid-midstance detection using toe distance. Dashed red line shows algorithmically calculated mid-midstance. Solid black line shows actual frame number of the mid-midstance.

As shown in the Figure 4.8, the algorithm estimated mid-midstance a few frames before the actual mid-midstance, and there were several false positives. Therefore, a different approach that measured the distance between the left and right big toe keypoints was used. As shown in Figure 4.9, the toe distance approach calculates mid-midstance more accurately than the knee distance approach.

Coronal view

For a coronal view, the beginning and end of the stride, and mid-midstance must be located. The same procedure was used as in the sagittal view, measuring the distance between the toes. The midhip forward distance from the heel keypoints at its maximum was used to detect the first heel strike (i.e., start of the current gait cycle) and the following heel strike by the same leg, which gives the end of the current gait cycle and the start of the next gait cycle. Heel strike detection for the right and left legs are shown in Figure 4.11. The algorithm-based heel strike differed greatly from the ground truth foot strike due to limitations in OpenPose's identification of foot keypoints, particularly the heel, ankle, and small toe keypoints. In the coronal view, these keypoints tend to cluster, overlap, or get obstructed by the big toe keypoint. Additionally, OpenPose faces challenges in accurately identifying the keypoints of the heel and small toe when the person appears smaller in the video frame as they move farther away from the camera (Figure 4.10)

Figure 4.10 Four foot keypoints overlapping.

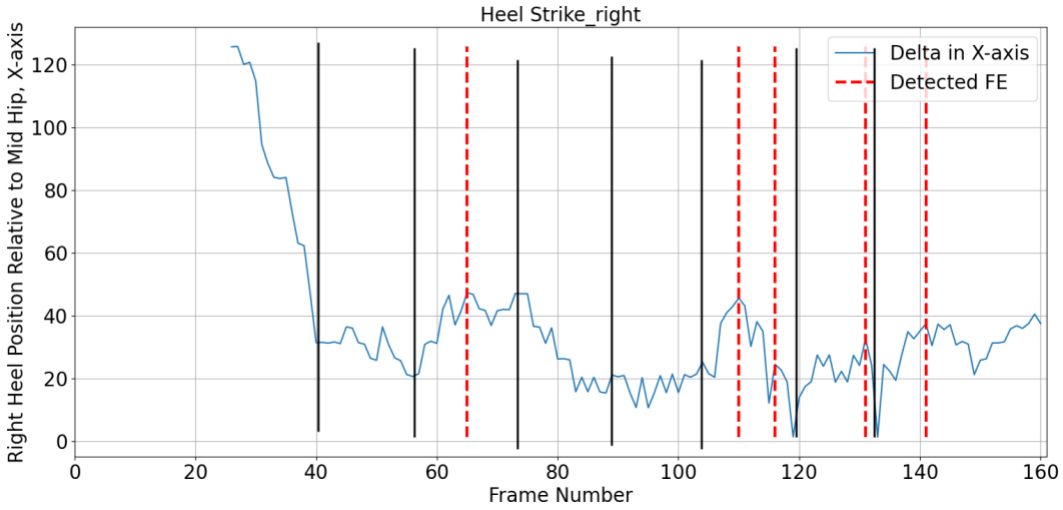

(a)

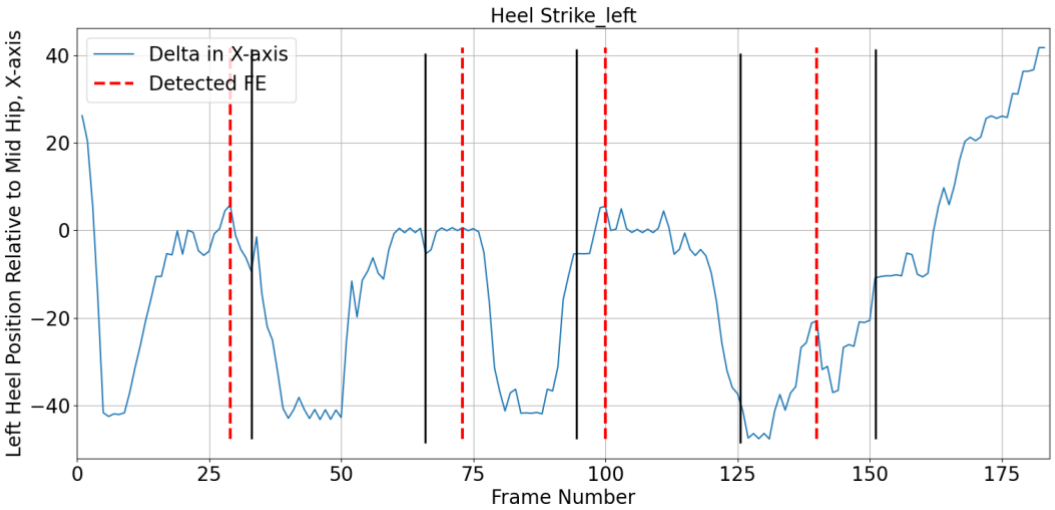

(b)

Figure 4.11 Heel strike identification for right (a) and left leg (b) using the distance between mid-hip keypoint and the heel keypoint. The dashed red line shows the algorithmically calculated heel strike, whereas the solid black line shows actual frame number of the heel strike.

The distance between the toes method was then used to determine mid-midstance, as well as the beginning and end of strides. This approach was used since OpenPose consistently identified the big toes, even when the person was further away from the camera. When the distance is smallest, the toes are close to each other, resulting in mid-midstance. When the distance is the largest, the toes are far apart, resulting in heel strike. In comparison to the previous approach, this approach predicted heel strike more accurately (Figure 4.12).

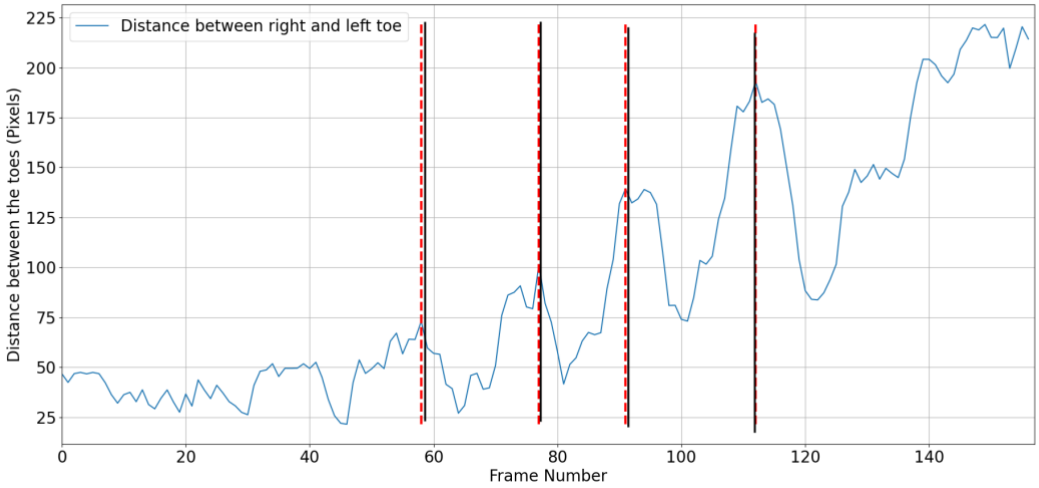

(a)

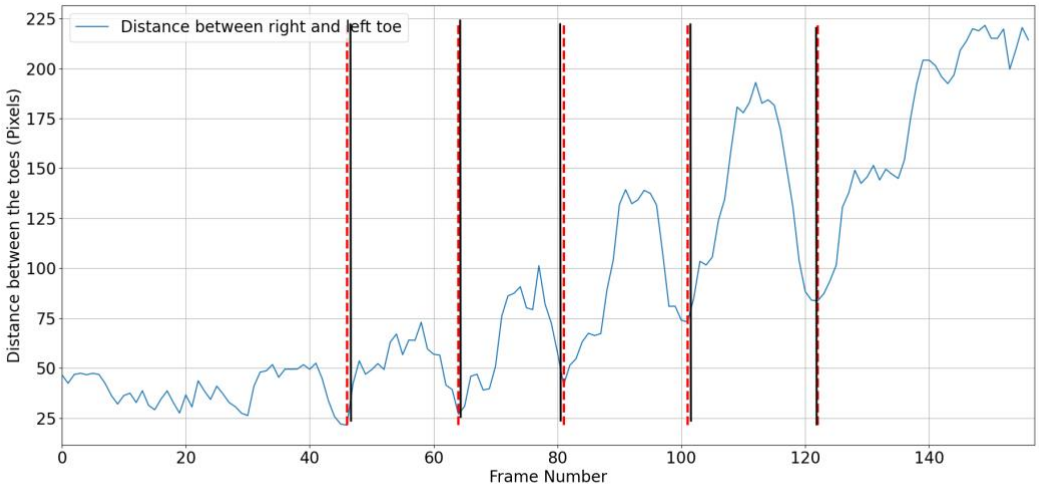

(b)

Figure 4.12 Distance between the toes during a walking trial (a) heel strike and (b) mid-midstance. The red dashed line is algorithm's estimated mid-midstance and heel strike. Solid black lines are ground truth for mid-midstance and heel strike.

4.2.3 Allocating foot events to specific strides

Figure 4.13 provides a flowchart for identifying strides. Following these steps, foot events are assigned to particular strides by determining if the stride begins on the left or the right, acquiring at least a stride to determine if the number of right/left foot strikes equals or exceeds 2, and assigning events to particular strides by searching for foot-strikes, foot-offs, or mid-midstance that

could happen between the start and finish of the stride. If there are fewer 2 foot-strikes, the warning "insufficient number of strikes" will appear at the end of the loop.

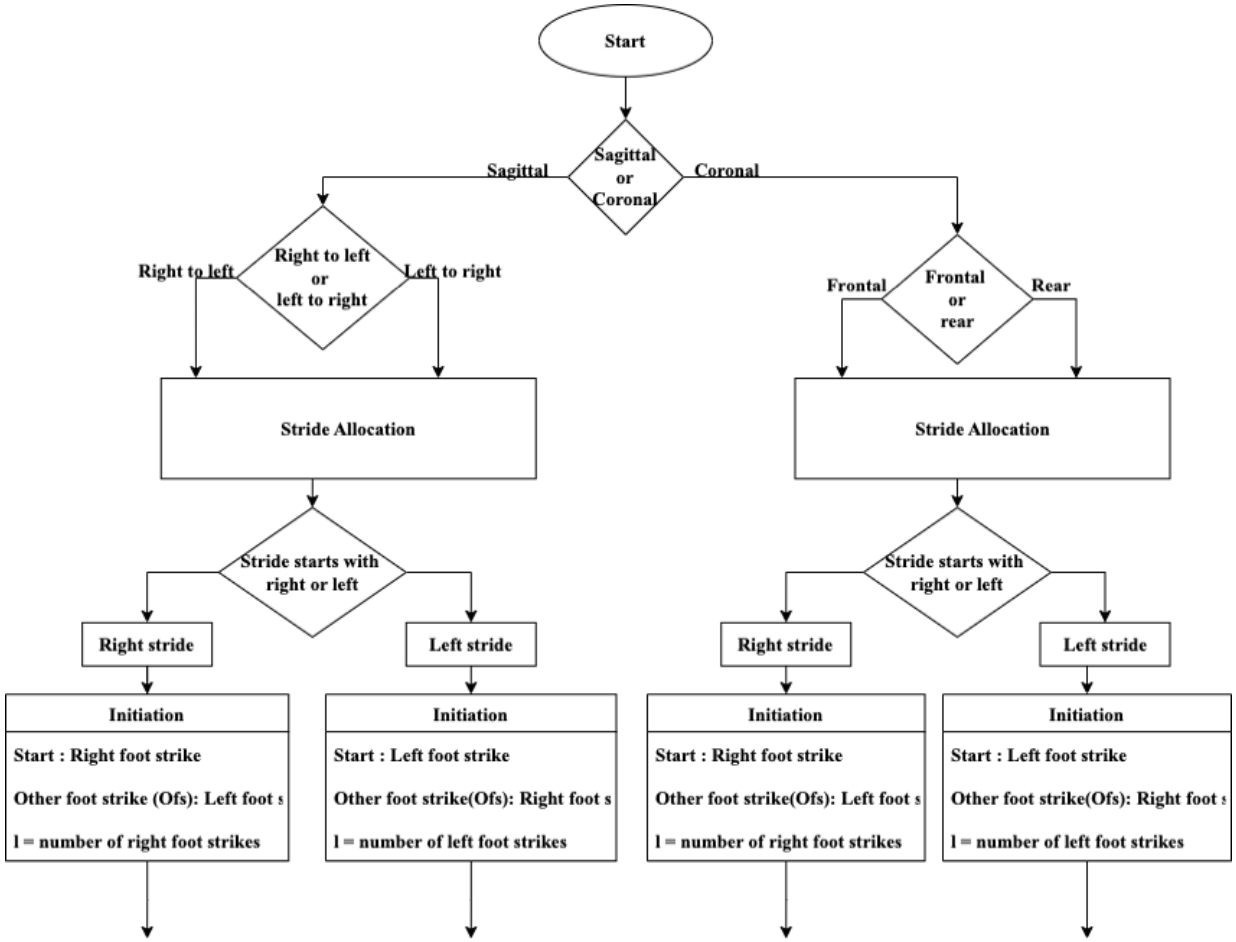

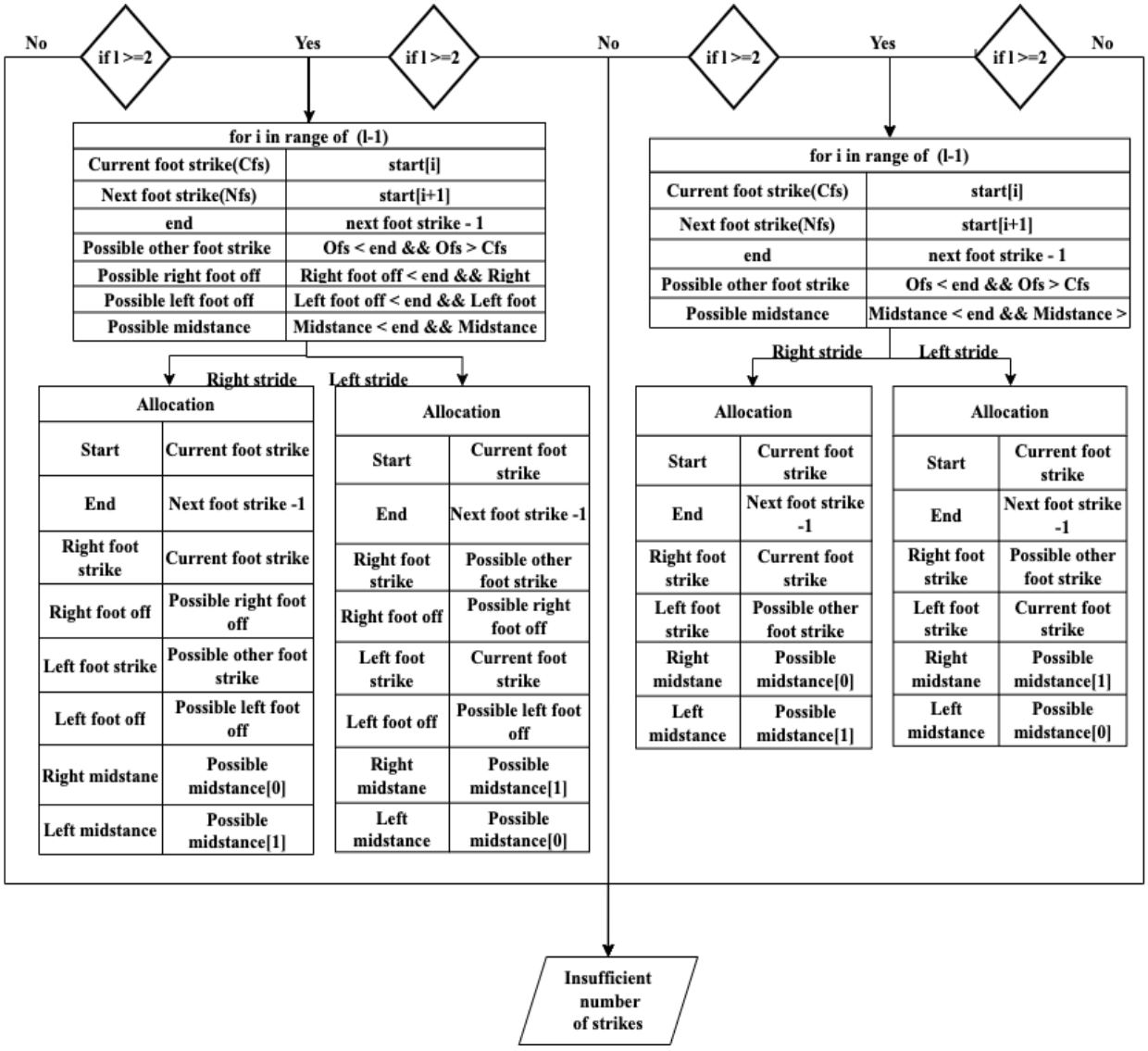

Figure 4.13 Flowchart of gait event identification

4.3 Algorithmic implementation of EVGS

The algorithmic implementation of the EVGS parameters is presented in the same order as the EVGS parameters were presented in Chapter 3.

4.3.1 Peak hip flexion in swing (#13)

To determine hip angle, the angle between the axis perpendicular to the trunk axis and the thigh axis was computed in the sagittal plane, since OpenPose does not provide keypoints for a pelvis segment. The trunk axis was the axis between the neck and mid-hip keypoints. The line connecting the hip and knee keypoints was the thigh axis. Note that this is different from how people can

visualize hip angle, which is usually the thigh angle related to pelvis orientation.

Equation 4.2 was used to calculate the slope:

$$m = \frac{y_2 - y_1}{x_2 - x_1} \tag{4.2}$$

For the trunk axis, (x_1, y_1) are the neck coordinates and (x_2, y_2) are the mid-hip coordinates. Using these coordinates and equation 4.2, the trunk axis angular coefficient was determined. The axis perpendicular to the trunk axis thus had the following slope:

$$m_1 = \frac{1}{m} \tag{4.3}$$

A similar procedure was followed for the thigh axis, where m_2 was calculated from (x_3, y_3), which corresponds to the hip's coordinates, and (x_4, y_4) represents the knee keypoints.

$$m_2 = \frac{y_4 - y_3}{x_4 - x_3} \tag{4.4}$$

Therefore, the angle (in degrees) is given by

$$\theta_{hip} = 90 - arctan \left\| \frac{m_2 - m_1}{1 + (m_2 * m_1)} \right\| * \frac{360}{2\pi} \tag{4.5}$$

When the knee is in front of the body, the angle value is positive (flexion).

4.3.2 Knee extension in terminal swing (#10)

Knee extension in terminal swing is determined using the knee angle. The knee angle is between the thigh and shank sagittal axes. When the knee is flexed, the angle is positive. Equation 4.4 determines the slope of the thigh segment and equation 4.6 is for the tibia segment slope.

The axes used to compute joint angles are shown in Figure 4.14.

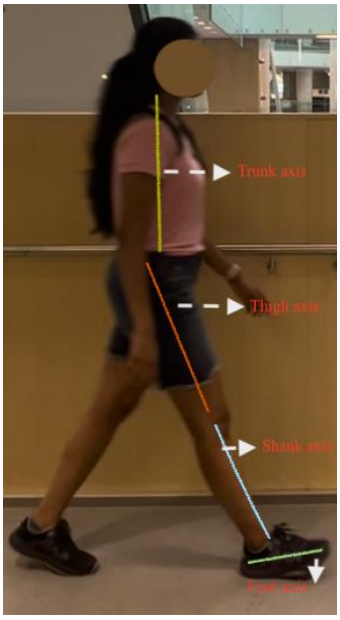

Figure 4.14 Axes for EVGS computation

For the thigh, hip coordinates were (x_3, y_3), and knee coordinates were (x_4, y_4) and equation 4.4 is used to compute the angular coefficient of thigh axis m_2.

The ankle coordinates were (x_5, y_5). The slope, m_3, was calculated using equation 4.6.

$$m_3 = \frac{y_5 - y_4}{x_5 - x_4} \tag{4.6}$$

Knee angle was then calculated using

$$\theta_{knee} = arctan \left\| \frac{m_3 - m_2}{1 + (m_3 * m_2)} \right\| * \frac{360}{2\pi} \tag{4.7}$$

4.3.3 Initial contact (#1)

To determine whether the heel, toe, or flatfoot makes initial contact with the ground, a line (foot axis) between the heel and mid-toe (midpoint of the large and small toes) keypoints were used. The angle between the foot axis and the image coordinate system x-axis in sagittal plane was measured. The development dataset was used to calculate angle thresholds for scoring. The thresholds were determined by evaluating sagittal videos showing any of the three conditions (heel contact, toe contact, flatfoot contact). After analysis, the flatfoot contact range was set to between 0° and 20° since 95% of the development dataset showed heel contact at more than 20° and toe contact less than 0°.

4.3.4 Peak sagittal trunk position (#16)

Similar to the foot position approach, a line from the neck to the mid-hip keypoint was used for trunk angle. The angle between this trunk line and the x-axis of the image coordinate system in the sagittal plane was calculated. Then, in accordance with the EVGS handbook [15], normal (vertical to 5° forward or backward), abnormal (greater than 5° backwards or between 6° and 15° forward), and highly abnormal (more than 15° forward) conditions were classified.

4.3.5 Pelvic rotation in midstance (#15)

OpenPose only provides hip keypoints, but the pelvis requires at least 3 keypoints to define segment orientation. As a surrogate measure, pelvic rotation angle is determined from a line connecting the right and left hip joints and the image coordinate system's sagittal plane y-axis.

4.3.6 Heel lift (#2)

Heel lift has five EVGS criteria: normal, early, delay, no heel, and no forefoot contact. Using the same methodology for detecting foot position at initial contact, no forefoot touch and no heel contact are detected at midstance. "No forefoot contact" refers to when the forefoot (the front part of the foot, including the toes) does not contact the ground during mid-stance. "No heel contact" refers to when the heel does not contact the ground during mid-stance.

Three foot-events (stance foot heel lift, other foot level with the stance foot, opposite foot contact with the ground) are recorded if the foot is in a flat posture during midstance. A normal EVGS score occurs if heel lift occurs on the stance leg between the other foot being at the same level as the stance foot and the other foot making contact with the ground. Heel lift is early if the stance leg heel lift occurs before the opposing foot levels with the stance foot. Heel lift is delayed if lifting occurs after the opposing foot reaches the ground.

4.3.7 Peak hip extension in stance (#12)

Peak hip extension is determined by calculating hip angle in stance using equation 4.7.

4.3.8 Peak knee extension in stance (#9)

Similar to the knee extension in terminal swing, this parameter is calculated using the knee angle given in the equation 4.7.

4.3.9 Maximum ankle dorsiflexion in stance (#3)

The angle between the foot axis and the shank sagittal axis is dorsiflexion/plantarflexion. Dorsiflexion angles are positive. Equations 4.8 and 4.9 are used to determine the tibia and foot segments. The knee coordinates are (x_4, y_4), and ankle coordinates are (x_5, y_5). Using equation 4.6, the angular coefficient is m_3.

The heel coordinates are (x_6, y_6) and the mean positions of the first and fifth toes are (x_7, y_7). Equation 4.8 determines the slope m_4.

$$m_4 = \frac{y_7 - y_6}{x_7 - x_6} \tag{4.8}$$

The ankle angle is calculated using equation 4.9.

$$\theta_{ankle} = arctan \left\| \frac{m_4 - m_3}{1 + (m_4 * m_3)} \right\| * \frac{360}{2\pi} \tag{4.9}$$

4.3.10 Peak knee flexion in swing (#11)

Similar to the knee position and knee extension parameter, this parameter is derived using the knee angle given in equation 4.7.

4.3.11 Maximum ankle dorsiflexion in swing (#7)

This is similar to the maximum ankle dorsiflexion parameter in stance (#3). Ankle angles were calculated using equation 4.9. The main difference is that the previous maximum ankle dorsiflexion parameter used a terminal stance frame, while “maximum ankle dorsiflexion in swing” uses a midswing frame

4.3.12 Foot clearance in swing (#6)

Foot clearance has four criteria: full clearance, reduced clearance, no clearance, and high steps. Toe, heel, and ankle keypoints are considered for this parameter. Full clearance occurs when the toe and heel involved in foot clearance cross the toe and heel of the opposing leg, respectively. Reduced clearance occurs when the heel crosses the opposing leg's heel, but the toe remains below or on the same level as the opposite leg's toe. No clearance is when both toe and heel are below the opposite toe and heel, respectively. A high step occurs if the toe passes the opposite leg's midpoint between the ankle and knee.

4.3.13 Maximum lateral trunk shift (#17)

The EVGS instructions for maximum lateral trunk shift are not machine-friendly because the scale's description only refers to "marked," "reduced," or "moderate" trunk shift, with no threshold values provided to distinguish between the various conditions. The proposed approach for determining lateral trunk shift involves computing the angle between the trunk axis and the image coordinate's y-axis in the coronal plane. Angle thresholds at which the trunk shift is normal, moderate, and marked were determined using the development dataset. Videos from the coronal view that displayed any of the three conditions (normal, mild trunk shift, marked trunk shift) were analyzed. After analysis, maximum lateral trunk shift was considered normal if the angle was between 0° and 5°, reduced if the angle was less than zero, moderate if the trunk angle was between 6° and 15°, and severely inclined if the trunk angle was greater than 15°.

4.3.14 Maximum pelvic obliquity in midstance (#14)

Similar to pelvic rotation, pelvic obliquity angle is determined between a line connecting the right and left hip joints and the image coordinate system's y-axis in the coronal plane.

4.3.15 Knee progression angle (#8)

Knee progression angle is highly subjective and depends on visual cues. This parameter determines if the kneecap is visible. EVGS instructions are insufficient to determine the knee progression angle using only OpenPose keypoints. The proposed method of determining knee progression angle involves obtaining the ankle angle using equation 4.9 and establishing threshold values using the development dataset. Following video analysis, normal was chosen as an ankle angle between -25º to 25º, internal rotation as an ankle angle more than 25º, and external rotation as an ankle angle less than - 25º.

4.3.16 Foot rotation (#5)

The ankle angle given in equation 4.9 is used to determine foot rotation.

4.3.17 Hindfoot valgus/varus (#4)

Hindfoot valgus/varus is calculated using a line connecting the ankle and heel keypoints and the image coordinate's y-axis in the coronal plane.

5 Algorithm Evaluation: Methodology, Results and Discussion

This chapter presents the methodology to evaluate the new EVGS algorithmic scoring approach. Since the clinical implementation of EVGS is human-scored, algorithmic scoring was evaluated by comparison to scoring by a panel of scorers. This chapter is divided into three sections. The first section details the methodology for evaluating the algorithm, including the video collection process, the role of human scorers and their training, and how the comparison of scorer scoring with algorithmic scoring was implemented. The second section presents the results of the evaluation, while the third section presents and discusses the findings from these results.

5.1 Methods

5.1.1 Video data set

To develop the algorithm, a preliminary set of videos was collected. These videos featured an able-bodied individual walking in both sagittal and coronal views, and were captured using a handheld smartphone camera operating at a 60 Hz.

To assess automated EVGS analysis system performance, a separate set of videos was collected. This set included videos depicting both normal and abnormal gait conditions for each EVGS parameter (i.e., the person walked to match conditions for each EVGS parameter). This also allowed for a thorough evaluation of the system performance since the videos can be used to test various gait patterns.

Participant recruitment

Three participants volunteered from the Mobile Motion Lab, a collaboration between the Children's Hospital of Eastern Ontario (CHEO) clinicians and University of Ottawa professors and students. The participants had a solid understanding of gait events. Participants were instructed to wear running shoes; tightly fitting, brightly colored clothes; and shorts with kneecap visible. Participants were female, 20 to 25 years, and with no issues affecting walking. Inclusion criteria were being an able-bodied individual and having the ability to follow instructions.

Data collection strategy

Before video recording, the gait conditions mentioned in the EVGS scale were explained to

participants so that they could recreate these conditions. Nine gait sets were collected for the sagittal view (healthy, hip, knee, trunk, ankle, pelvis, foot position, heel lift, foot clearance) (Table 5.1) and five gait sets for the coronal view (healthy, knee, trunk, foot, pelvis) (Table 5.2). Thirty-seven walking trials were collected, one for each condition and two were normal gait. This approach allowed for a comprehensive examination of different gait conditions and can help in the evaluation of algorithms for automatically calculating EVGS.

Table 5.1 Gait sets in sagittal view

Gait set	Condition	Description
Healthy	Normal	Walk normally
Hip	Flexion Extension	At initial contact, walk with your hips flexed. At terminal stance, walk with your hips extended.
Knee	Flexion Extension	At initial contact and mid-swing, walk with your knee flexed. At initial contact and terminal stance, walk with your knee extended.
Ankle	Dorsiflexion Plantarflexion	During terminal stance and mid-swing, walk with your ankle dorsiflexed. During terminal stance and mid-swing, walk with your ankle plantarflexed.
Trunk	Reduced Moderate Marked	Walk with your trunk more than 5° backward. Lean forward 6° to 15° while walking. Lean more than 15° forward while walking.
Pelvis	Protraction Retraction	Walk with the pelvic region extended more than 10°. Retract the pelvic region more than 5° when walking.
Foot position	Toe contact Heel contact Flatfoot contact	Make initial contact with the floor with your toes. Make initial contact with the floor with your heel. Make initial contact with the ground with foot flat.
Heel lift	No forefoot contact No heel contact Early Delayed	Walk on your heel. Walk on your toes. Raise your heel off the ground before your opposing foot aligns with your stance foot. Raise your heel from the ground after the opposing foot has contacted the ground.
Foot clearance	High steps Reduced clearance No clearance	Lift your knees high in the air as you walk. Do not completely lift your foot off the ground as you walk. Either the heel or toe is still in contact with the ground. Do not take your feet off the ground. When walking, drag your legs.

Table 5.2 Gait sets in coronal view

Gait set	Condition	Description
Healthy	Normal	Walk normally
Knee	External: Full kneecap	Walk with your knees externally rotated and your whole kneecap visible
	External: Part kneecap	Walk with your knees externally rotated and your part of the kneecap visible
	Internal: Full kneecap	Walk with your knees internally rotated and your whole kneecap visible
	Internal: Part kneecap	Walk with your knees internally rotated and your part of the kneecap visible
Foot	External: Moderate	Walk with your feet 21° to 40° externally rotated.
	External: Marked	Walk with your feet turned externally by more than 40°.
	Internal: Marked	Walk with your feet 1° to 25° internally rotated.
	Internal: Moderate	Walk with your feet internally rotated by greater than 25°.
Pelvis	Up	When you walk, lift one hip over the other by more than 5°.
	Down	When walking, lower one hip more than a degree while raising the other.
Trunk	Reduced	During midstance, walk with your trunk tilted toward the opposing leg.
	Moderate	Tilt your trunk more than 25 millimeters toward the stance leg at midstance.
	Marked	At midstance, lean your trunk significantly towards the stance leg

Setup and video collection

Data were collected using an iPhone 13 pro with 2532x1170 pixel resolution. The videos were captured in 1080p resolution at 60 frames per second (fps).The smartphone was handheld to replicate use situations without a tripod or other support. Three individuals were involved in each recording process: a volunteer being recorded, a phone video recording operator, and an assistant to monitor the recording. The operator was instructed to maintain a steady hand and hold the camera at approximately neck level during the entire trial, to ensure that the participant's entire body was captured in the video. The camera was oriented parallel to the plane being captured (i.e., sagittal or coronal). For the coronal view, the operator positioned themselves in front of the participant as they walked towards the camera. The participant then turned around and walked away from the camera. In the sagittal view, the operator stood to the side of the participant to capture their entire side body. The participant walked from left to right, covering a minimum of three strides, and then reversed direction, walking from right to left. The distance between the participant and video operator varied was based on the participant's body height, such that the body was within the video field while being as large as possible (Figure 5.1).

A satisfactory video had the participant visible, balanced indoor lighting, and no images, objects, or people in the background that may be mistaken for the participant. The recording took place in a university corridor with tile flooring as the surface and without other people walking in the capture area. The walls and floor were bare.

A brief description, diagram, or video of each gait pattern was provided before the video trial to ensure that the participants understood and interpreted the walking pattern correctly. Additionally, a manual was provided for the participants to read before the video session, to help reduce any bias that may be introduced by any demonstration of the gait pattern.

During each trial, participants were instructed to walk a minimum of three strides at a comfortable self-selected speed in the hallway. After completing the initial strides, participants took a brief two-second break, then turned 180° in their chosen direction, followed by another brief two-second break. Subsequently, participants resumed walking straight for least three additional strides. To achieve the required stride count, a distance of 10 meters was sufficient. Each participant completed 37 walking trials, resulting in 111 videos being collected.

Video processing

To ensure the quality and consistency of the video data, pre-processing steps were carried out on the collected dataset. Each video was trimmed at the start and end to eliminate frames where the person was not on camera. Sagittal view videos were divided into left to right and right to left directions, while coronal view videos were divided into front view and rear view. Video quality was checked to ensure that it met the required standards. Videos that were not taken correctly were removed and recaptured.

After pre-processing, 216 videos were available for analysis.

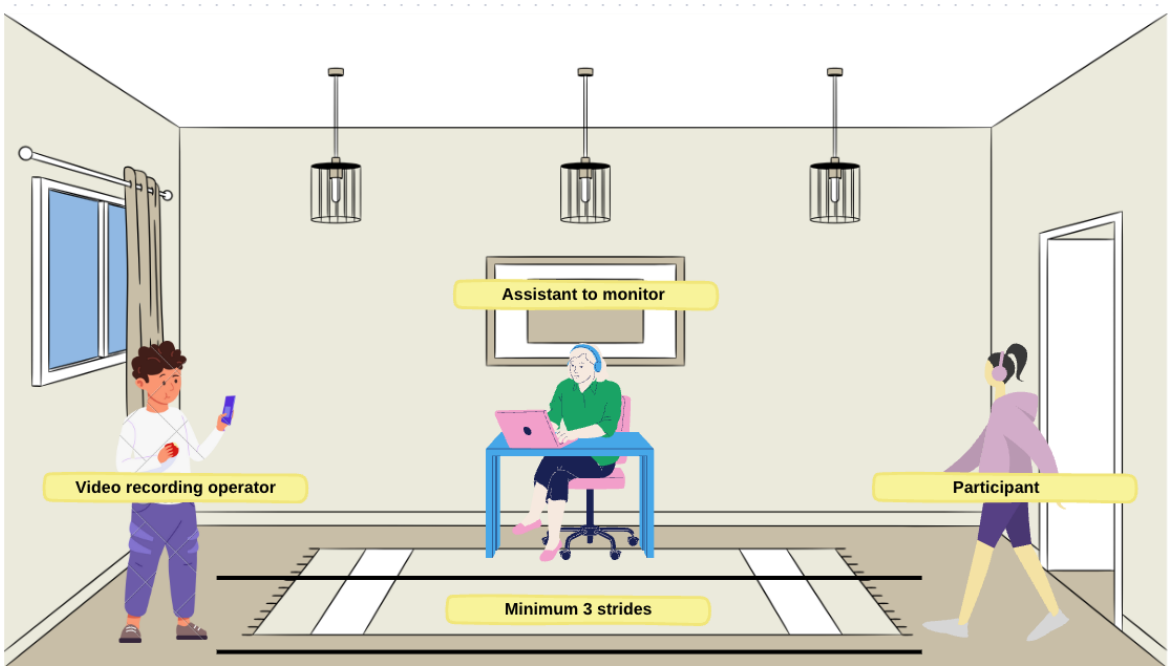

(a)

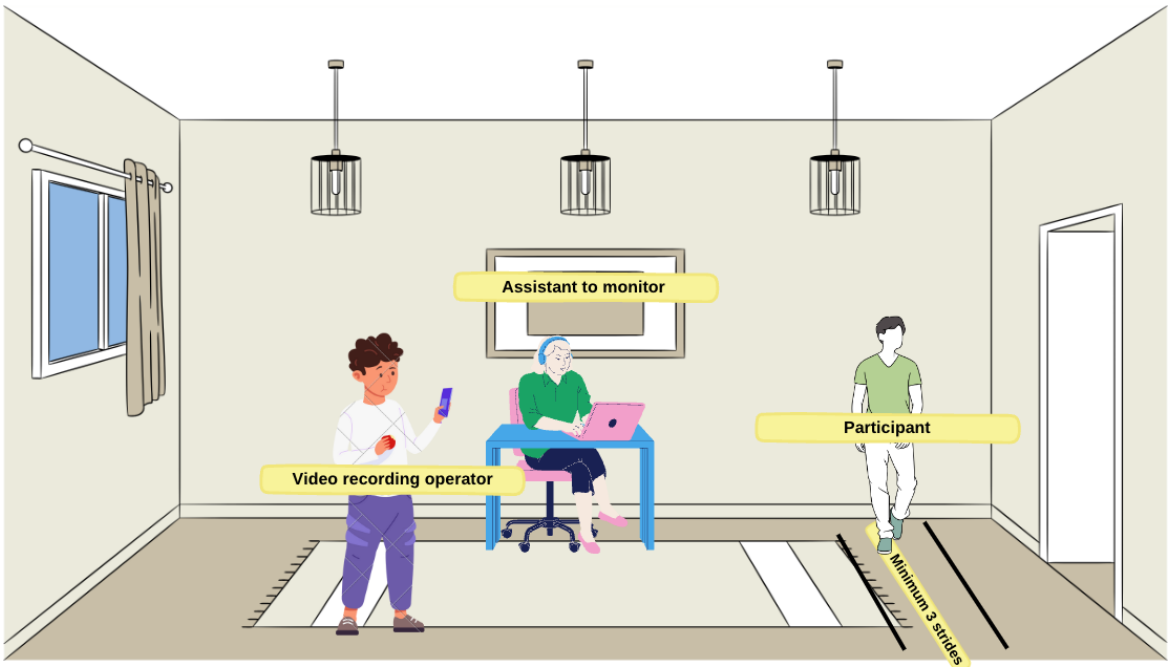

(b)

Figure 5.1 Setup for video recording in both sagittal (a) and coronal (b)views

5.1.2 Scorers and training

In clinical settings, the Edinburgh Visual Gait Score (EVGS) is a score assigned by a human through video observation of a person's walking. To assess algorithm performanc scores by humans were compared with the scores generated by the algorithm.

Five University of Ottawa students who were Mobile Motion Lab team members volunteered to score videos, each with a sufficient understanding of gait events but little expertise in EVGS. Before evaluating the videos, all scorers were briefed on normal gait kinematics, gait phases, and methodologies for recording and reviewing gait recordings. Additionally, the purpose and background of the EVGS were discussed, and gait analysis using the EVGS was demonstrated.

For training, the scorers manually scored an example video using the EVGS and then compared their results to gain a better understanding. The scorers then used EVGS to evaluate the video independently, without consulting one another. Slow motion and freeze-frame playback were used with video player software. Scorers did not have time restrictions and could work at their own pace while reviewing.

5.1.3 Algorithm evaluation methodology

To validate the approach to automatically calculate EVGS scores, independent evaluations were completed for stride detection and EVGS scoring.

To evaluate the stride detection algorithm, ground truth foot events were manually identify . One of the scorers thoroughly reviewed each video and manually identified the foot events. The ground truth was then manually labeled for coronal/sagittal view, motion direction, foot strike and foot off, mid-midstance, and the total number of strides in each video. For EVGS algorithm evaluation, each video was scored by at least two scorers. The scorers used the EVGS to evaluate the videos independently, without consulting one another. Each scorer was unaware of the other scorer’s results.

Each scorer completed an EVGS form containing all the EVGS parameters for each leg. The scorers evaluated the entire gait cycle, including multiple strides, for each leg in each video. However, only the most frequent score (aggregate score) for each parameter for each leg in each video was considered as the final score. The use of an aggregated score also helped reduce potential biases introduced by evaluating only a single stride, The videos are rated between 0 and 2, with 0

denoting normal performance and two denoting highly abnormal as given in EVGS scale. Scorers were instructed to assess joint angles using their eyes alone, without using any software or other tools, to replicate the instructions described in EVGS.

Once the ground truth for coronal/sagittal view, motion direction, foot strike and foot off, mid-midstance, the total number of strides and the EVGS score was marked by the scorers for each video, the algorithmic results and EVGS scores were compared with the scorer results. When using a human-scored scale like the EVGS, it is important to assess the degree of agreement or disagreement between different scorers. One way to do this is to perform a correlation analysis between the scores assigned by different scorers, which can help to determine the degree of consistency. Pearson correlation is a statistical measure that is used to evaluate the strength and direction of the linear relationship between two variables. In this case, the correlation was used as a metric to compare algorithmic and scorer results.

5.2 Results

The outcomes of each step in gait event and stride detection (view detection, direction of motion detection, gait event identification, and stride allocation) are reported in Section 5.2.1. The evaluation of gait event and stride detection involved comparing the algorithmic findings with the scorer marked ground truth. In Section 5.2.2, the results of each EVGS parameter are presented. For EVGS, the correlations between the scorers and the correlations between the algorithmic scores and each scorer (scorer 1 and scorer 2) are reported.

5.2.1 Results of foot event and stride detection

Coronal/Sagittal view detection

To assess sagittal or coronal view identification, algorithmic findings and ground truth were compared. Table 5.3 displays sagittal or coronal view (number of videos) classification confusion matrices. The accuracy was 96.3%, sensitivity was 93.1%, specificity was 98.4%, precision was 97.6%, and F1-score was 0.95.

Table 5.3 Confusion matrix for coronal/sagittal view identification

Algorithm / Ground Truth	Coronal	Sagittal
Coronal	82	2
Sagittal	6	126

Algorithm accuracy was acceptable. However the algorithm mistakenly identified the video as frontal coronal in some instances when multiple people were in the video or a person unexpectedly turned towards the camera while walking in the sagittal view (i.e., person's orientation changed towards the camera).

Motion direction detection

Table 5.4 and Table 5.5 show confusion matrices for detecting the direction of motion (number of videos). For the coronal view, accuracy was 92.8%, sensitivity was 90.9%, specificity was 95.0%, precision was 95.2%, and F1-score was 0.93. For the sagittal view, accuracy was 92.4%, sensitivity was 93.7%, specificity was 91.1%, precision was 90.9%, and F1-score was 0.92.

Table 5.4 Confusion matrix for detecting direction of motion (coronal view)

Algorithm / Ground Truth	Frontal	Rear
Frontal	40	2
Rear	4	38

Table 5.5 Confusion matrix for detecting direction of motion (sagittal view)

Algorithm / Ground Truth	Left	Right
Left	60	6
Right	4	62

The algorithm correctly determined direction in the majority of videos. The algorithm failed to properly detect when a person's reflection was visible on the wall, when numerous people were in the video, when the camera moved as the person moved (both small and large movements of the camera), or when the participant was not in the frame the entire time.

Foot strike, foot off, and mid-midstance detection

The algorithmically determined foot strike, foot off, and mid-midstance were compared to manually labelled ground truth. Each video was classified into three categories based on the discrepancy between the identified frame number and the actual frame number. The categories were: two frames or less discrepancy, two to five frames discrepancy, and more than five frames discrepancy. Each stride was marked and the most frequently occurring category was recorded as the final result. Figure 5.2 shows an example in which the algorithm identified foot events within two frames of the ground truth.

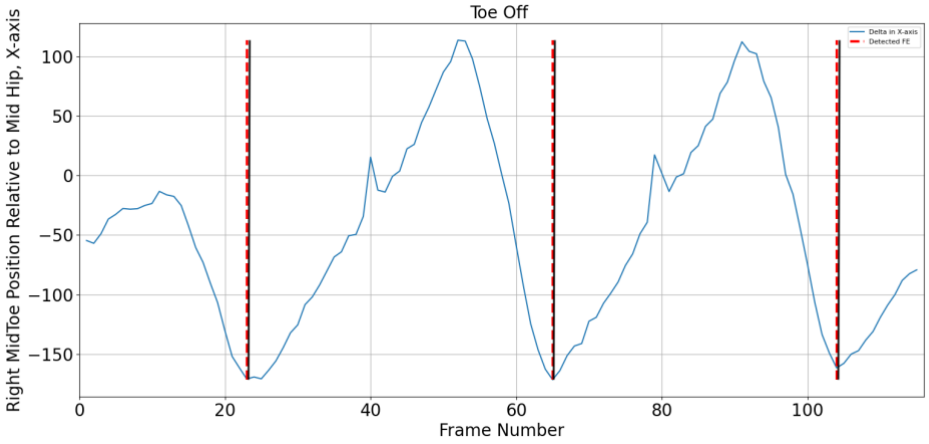

(a)

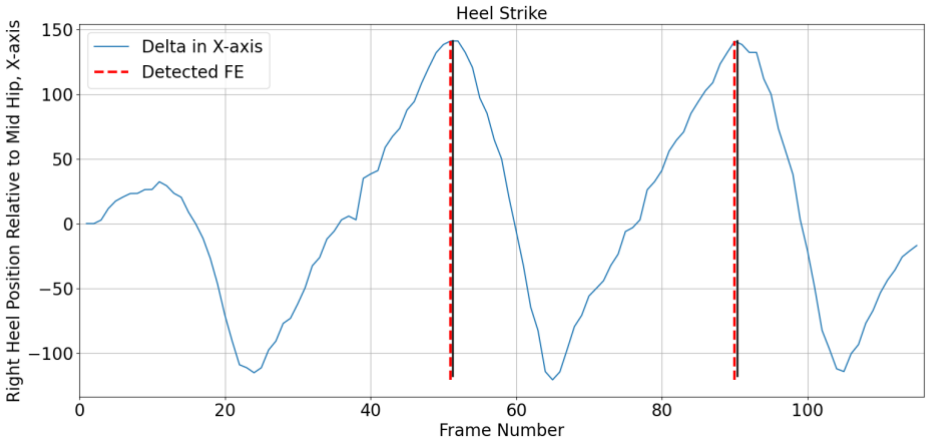

(b)

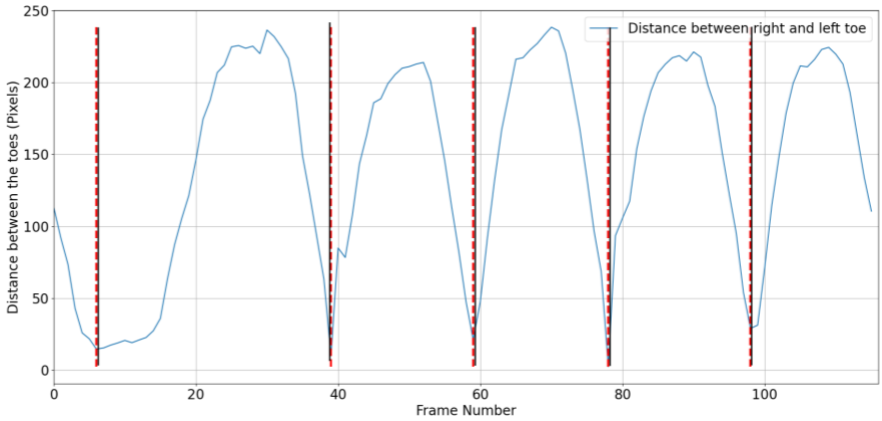

(c)

Figure 5.2 Example where the algorithm detects a (a) toe-off (b) heel strike and (c) mid-midstance (shown by a dashed red line) within two frames of a manually labeled event (solid black line).

Additional foot events may occasionally be detected by the algorithm, while other times the algorithm may not detect an event. These circumstances occurred only on rare times when the OpenPose keypoints abruptly swapped between legs. Figure 5.2 (a) shows an example in which the algorithm finds additional mid-midstance, while Figure 5.2 (b) shows an example in which the algorithm failed to recognise midstance.

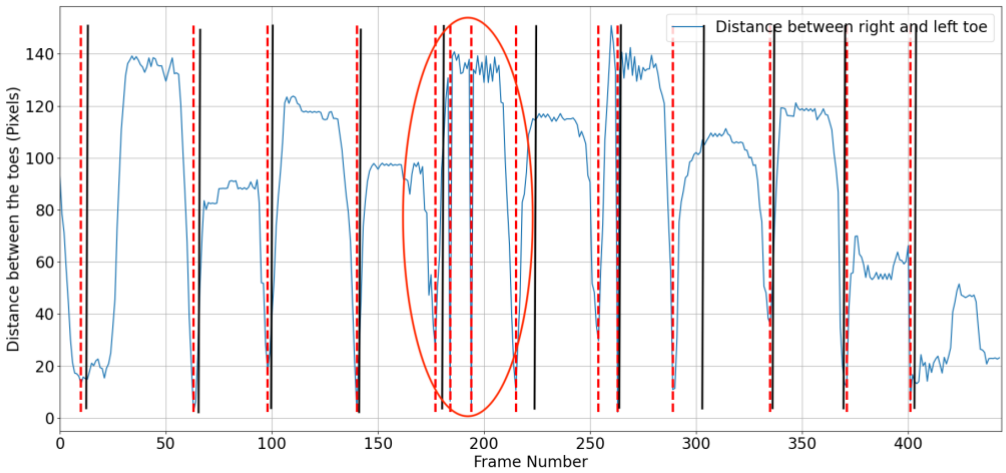

(a)

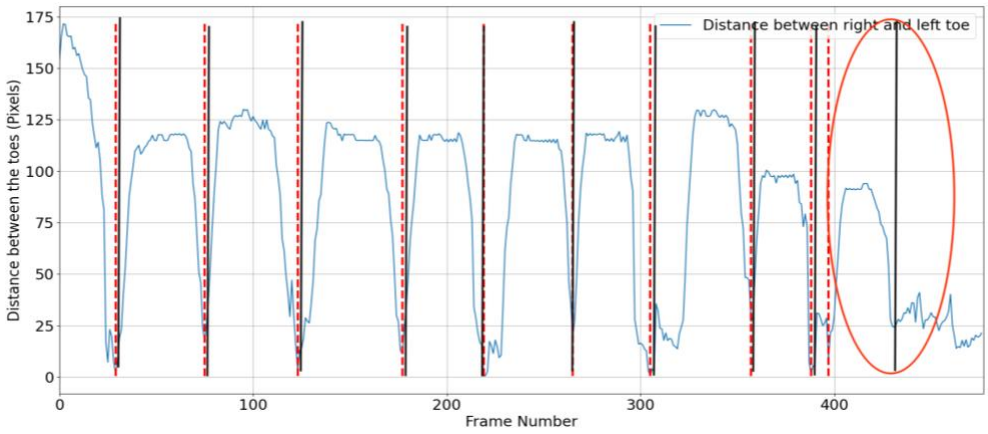

(b)

Figure 5.3 An example of a scenario in which the algorithm detects additional mid-midstance (a) but fails to detect a mid-midstance (b) (shown by ellipse region).

Table 5.6, Table 5.7 and Table 5.8 compare foot strike, foot off, and mid-midstance.

Table 5.6 Foot strike accuracy. The number of videos in each category in sagittal or coronal views.

	Differ by more than five frames	**Differ by two to five frames**	**Differ by Two frames or less**
Coronal	22	27	35
Sagittal	20	91	21

Table 5.7 Foot off accuracy. The number of videos in each category in sagittal or coronal views.

	Differ by more than five frames	**Differ by two to five frames**	**Differ by Two frames or less**
Coronal	20	33	31
Sagittal	19	87	26

Table 5.8 Mid-midstance accuracy. The number of videos in each category in sagittal or coronal views.

	Differ by more than five frames	**Differ by two to five frames**	**Differ by Two frames or less**
Coronal	18	24	42
Sagittal	4	1	127

Number of strides

The difference between the number of strides detected by the algorithm and the number of strides detected by the scorer are displayed in Table 5.9. Each video was classified into three categories based on the difference between the identified number of strides and the actual number of strides. The categories were: two strides or less, two to five strides, more than five strides.

Table 5.9 Difference between the number of strides detected by the algorithm and the number of strides detected by the scorer

	Differ by more than five strides	**Differ by two to five strides**	**Differ by two strides or less**
Coronal	3	4	77
Sagittal	3	3	126

5.2.2 Results of automated Edinburgh Visual Gait Score

Coronal videos

EVGS scores were computed for five coronal view parameters. Pearson correlation analyses assessed the relationship between scorer 1 and scorer 2, scorer 1 with the algorithm, and scorer 2 with the algorithm, for both legs for each gait set. EVGS score correlations between scorers (R1,

R2) and the algorithm for right and left legs for different gait sets are shown in separate tables: Table 5.10 for healthy gait set, Table 5.11 for the knee gait set, Table 5.12 for the foot gait set, Table 5.13 for the pelvis gait set, and Table 5.14 for the trunk gait set. Table 5.15 reports the overall average correlation between scorers and algorithm of entire dataset, as well as the average correlation of scorers for each parameter.

Table 5.10 EVGS correlations between scorers (R1, R2) and the algorithm for healthy gait set

Parameter	**R1 and R2**		**R1 and algorithm**		**R2 and algorithm**	
	Right	Left	Right	Left	Right	Left
Lateral trunk shift (#17)	1.00	1.00	0.84	0.61	0.84	0.61
Pelvic obliquity (#14)	0.92	1.00	0.92	1.00	0.84	1.00
Knee progression angle (#8)	1.00	1.00	0.92	1.00	0.92	1.00
Foot progression angle (#5)	1.00	1.00	1.00	0.83	1.00	0.83
Hindfoot valgus/varus (#4)	1.00	1.00	-0.61	-0.61	-0.61	-0.61

Table 5.11 EVGS correlations between scorers (R1, R2) and algorithm for knee gait set

Parameters	**R1 and R2**		**R1 and algorithm**		**R2 and algorithm**	
	Right	Left	Right	Left	Right	Left
Lateral trunk shift (#17)	0.52	0.77	0.77	0.62	0.67	0.81
Pelvic obliquity (#14)	0.52	1.00	-0.26	-0.26	-0.13	-0.26
Knee progression angle (#8)	0.45	0.67	0.70	0.92	0.87	0.87
Foot progression angle (#5)	0.92	1.00	0.77	0.83	0.83	0.64
Hindfoot valgus/varus (#4)	0.89	0.67	0.20	0.20	-0.04	0.30

Table 5.12 : EVGS correlations between scorers (R1, R2) and the algorithm for foot gait set

Parameters	**R1 and R2**		**R1 and algorithm**		**R2 and algorithm**	
	Right	Left	Right	Left	Right	Left
Lateral trunk shift (#17)	0.90	1.00	1.00	1.00	0.87	1.00
Pelvic obliquity (#14)	0.82	1.00	-0.58	0.58	0.71	0.58
Knee progression angle (#8)	0.58	0.58	0.58	0.58	0.33	1.00

Foot progression angle (#5)	1.00	1.00	1.00	0.90	1.00	0.90
Hindfoot valgus/varus (#4)	0.58	0.58	0.33	0.33	-0.58	-0.58

Table 5.13 EVGS correlations between scorers (R1, R2) and algorithm for pelvis gait set

Parameters	**R1 and R2**		**R1 and algorithm**		**R2 and algorithm**	
	Right	Left	Right	Left	Right	Left
Lateral trunk shift (#17)	0.70	0.29	0.77	0.45	0.54	0.22
Pelvic obliquity (#14)	0.92	0.67	0.60	-0.41	0.45	-0.31
Knee progression angle (#8)	0.88	0.71	0.45	0.10	0.22	0.49
Foot progression angle (#5)	0.49	0.61	0.27	0.71	0.91	0.06
Hindfoot valgus/varus (#4)	0.92	0.84	-0.38	0.38	0.54	0.38

Table 5.14 EVGS correlations between scorers (R1, R2) and algorithm for trunk gait set

Parameters	**R1 and R2**		**R1 and algorithm**		**R2 and algorithm**	
	Right	Left	Right	Left	Right	Left
Lateral trunk shift (#17)	0.72	0.84	0.75	0.64	0.60	0.50
Pelvic obliquity (#14)	0.87	0.78	0.10	0.64	-0.12	0.82
Knee progression angle (#8)	0.91	0.78	0.33	0.41	0.28	0.41
Foot progression angle (#5)	0.60	0.92	0.77	0.83	0.43	0.91
Hindfoot valgus/varus (#4)	0.68	0.68	0.22	-0.03	0.32	0.22

Table 5.15 The overall average correlation between scorers and algorithm of entire dataset, as well as the average correlation of scorers for each parameter.

	R1 and R2	**R1, R2 and Algorithm**		
Parameters		Right	Left	Average
Lateral trunk shift (#17)	0.77	0.77	0.65	0.71
Pelvic obliquity (#14)	0.85	0.25	0.34	0.30
Knee progression angle (#8)	0.76	0.56	0.68	0.62
Foot rotation (#5)	0.85	0.80	0.74	0.77
Hindfoot valgus/varus (#4)	0.78	-0.06	0.00	-0.03

Sagittal videos

The sagittal view had nine gait sets. Correlations between scorers (R1, R2) and the algorithm for right and left legs for different gait sets are shown in Table 5.16 for healthy gait set, Table 5.17 for the hip set, Table 5.18 for the knee set, Table 5.19 for the ankle set, Table 5.20 for the trunk set, Table 5.21 for the pelvis set, Table 5.22 for the foot position set, Table 5.23 for the heel lift set,and Table 5.24 for the foot clearance set. Table 5.25 reports the overall average correlation between scorers and algorithm of entire dataset, and the average correlation of scorers for each parameter

Table 5.16 EVGS correlations between scorers (R1, R2) and algorithm for healthy gait

Parameters	**R1 and R2**		**R1 and algorithm**		**R2 and algorithm**	
	Right	Left	Right	Left	Right	Left
Peak hip flexion (#13)	1.00	1.00	1.00	1.00	1.00	1.00
Knee extension in terminal swing (#10)	1.00	1.00	1.00	1.00	1.00	1.00
Initial contact (#1)	1.00	1.00	1.00	1.00	1.00	1.00
Peak sagittal trunk position (#16)	1.00	1.00	1.00	1.00	1.00	1.00
Pelvic rotation in midstance (#15)	1.00	1.00	0.69	0.71	0.92	0.98
Heel Lift (#2)	1.00	1.00	0.41	0.41	0.41	0.41
Peak hip extension (#12)	1.00	1.00	1.00	0.91	1.00	0.91
Peak knee extension in stance (#9)	1.00	1.00	0.92	0.87	0.92	0.87
Max ankle dorsiflexion in stance (#3)	1.00	1.00	1.00	0.75	1.00	0.75
Peak knee flexion in swing (#11)	1.00	1.00	1.00	1.00	1.00	1.00
Ankle dorsiflexion in swing (#7)	1.00	1.00	0.92	1.00	0.92	1.00
Foot clearance (#6)	1.00	1.00	-0.17	-0.24	0.17	-0.24

Table 5.17 EVGS correlations between scorers (R1, R2) and algorithm for hip set

Parameters	**R1 and R2**		**R1 and algorithm**		**R2 and algorithm**	
	Right	Left	Right	Left	Right	Left
Peak hip flexion (#13)	1.00	1.00	0.85	0.88	0.85	0.88
Knee extension in terminal swing (#10)	0.47	0.35	0.47	0.73	1.00	0.26
Initial contact (#1)	1.00	1.00	1.00	1.00	1.00	1.00
Peak sagittal trunk position (#16)	0.75	0.75	0.73	1.00	0.55	0.75
Pelvic rotation in midstance (#15)	1.00	0.91	0.73	0.93	0.73	0.88

Heel Lift (#2)	0.75	0.75	0.47	0.35	0.35	0.47
Peak hip extension (#12)	1.00	0.89	1.00	0.91	1.00	0.77
Peak knee extension in stance (#9)	1.00	1.00	0.92	0.87	0.92	0.87
Max ankle dorsiflexion in stance (#3)	0.68	0.68	0.55	0.75	0.37	0.11
Peak knee flexion in swing (#11)	0.55	0.55	0.55	0.73	1.00	0.40
Ankle dorsiflexion in swing (#7)	0.30	1.00	0.65	1.00	-0.26	1.00
Foot clearance (#6)	0.32	0.32	-0.11	0.24	-0.47	0.17

Table 5.18 EVGS correlations between scorers (R1, R2) and algorithm for knee gait set

Parameters	**R1 and R2**		**R1 and algorithm**		**R2 and algorithm**	
	Right	Left	Right	Left	Right	Left
Peak hip flexion (#13)	1.00	1.00	0.65	0.00	0.65	0.00
Knee extension in terminal swing (#10)	0.63	0.86	0.63	0.61	1.00	0.84
Initial contact (#1)	1.00	1.00	1.00	1.00	1.00	1.00
Peak sagittal trunk position (#16)	1.00	1.00	0.71	1.00	0.71	1.00
Pelvic rotation in midstance (#15)	0.71	0.71	-0.24	0.22	-0.34	0.46
Heel Lift (#2)	1.00	1.00	-0.32	-0.32	-0.32	-0.32
Peak hip extension (#12)	1.00	1.00	-0.20	1.00	-0.20	1.00
Peak knee extension in stance (#9)	1.00	1.00	1.00	0.88	1.00	0.88
Max ankle dorsiflexion in stance (#3)	0.82	0.82	0.27	1.00	0.50	0.82
Peak knee flexion in swing (#11)	0.63	0.63	0.45	0.61	0.71	0.77
Ankle dorsiflexion in swing (#7)	0.89	0.89	1.00	0.20	0.89	0.45
Foot clearance (#6)	-0.29	1.00	0.00	0.20	0.56	0.20

Table 5.19 EVGS correlations between scorers (R1, R2) and algorithm for ankle gait set

Parameters	**R1 and R2**		**R1 and algorithm**		**R2 and algorithm**	
	Right	Left	Right	Left	Right	Left
Peak hip flexion (#13)	1.00	1.00	1.00	1.00	1.00	1.00
Knee extension in terminal swing (#10)	1.00	1.00	1.00	0.77	1.00	0.77
Initial contact (#1)	1.00	1.00	1.00	1.00	1.00	1.00
Peak sagittal trunk position (#16)	1.00	0.71	0.71	1.00	0.71	0.71
Pelvic rotation in midstance (#15)	0.63	0.63	-0.43	0.71	-0.55	0.45
Heel Lift (#2)	0.88	0.88	-0.80	-0.80	-0.88	-0.88

Peak hip extension (#12)	1.00	0.71	0.63	0.50	0.63	0.71
Peak knee extension in stance (#9)	0.84	0.58	0.77	0.61	0.43	0.71
Max ankle dorsiflexion in stance (#3)	0.88	0.88	0.93	0.88	0.79	0.80
Peak knee flexion in swing (#11)	0.17	0.77	0.86	0.77	0.41	0.50
Ankle dorsiflexion in swing (#7)	1.00	1.00	1.00	1.00	1.00	1.00
Foot clearance (#6)	0.63	0.63	0.29	-0.25	0.00	-0.63

Table 5.20 EVGS correlations between scorers (R1, R2) and algorithm for trunk gait set

Parameters	**R1 and R2**		**R1 and algorithm**		**R2 and algorithm**	
	Right	Left	Right	Left	Right	Left
Peak hip flexion (#13)	0.82	0.67	-0.45	0.15	-0.46	0.23
Knee extension in terminal swing (#10)	0.89	0.70	1.00	0.75	0.89	0.67
Initial contact (#1)	0.81	0.81	1.00	0.86	0.81	0.78
Peak sagittal trunk position (#16)	1.00	1.00	0.82	0.82	0.82	0.82
Pelvic rotation in midstance (#15)	0.88	0.88	-0.45	0.01	-0.32	-0.02
Heel Lift (#2)	0.80	0.88	0.80	0.88	1.00	1.00
Peak hip extension (#12)	0.67	0.38	0.67	0.67	1.00	0.67
Peak knee extension in stance (#9)	0.68	0.50	0.75	0.90	0.75	0.43
Max ankle dorsiflexion in stance (#3)	0.80	0.80	0.91	1.00	0.49	0.80
Peak knee flexion in swing (#11)	0.49	0.38	0.90	0.82	0.30	0.31
Ankle dorsiflexion in swing (#7)	1.00	1.00	1.00	0.67	1.00	0.67
Foot clearance (#6)	0.55	0.94	-0.22	-0.16	-0.23	-0.17

Table 5.21 EVGS correlations between scorers (R1, R2) and algorithm for pelvis gait set

Parameters	**R1 and R2**		**R1 and algorithm**		**R2 and algorithm**	
	Right	Left	Right	Left	Right	Left
Peak hip flexion (#13)	0.61	0.17	0.58	-0.33	1.00	0.87
Knee extension in terminal swing (#10)	0.77	0.74	0.36	0.83	0.32	0.78
Initial contact (#1)	0.81	0.88	0.97	0.89	0.85	0.77
Peak sagittal trunk position (#16)	0.76	0.65	0.72	0.86	0.81	0.66
Pelvic rotation in midstance (#15)	0.56	0.43	0.22	0.27	-0.02	0.12
Heel Lift (#2)	0.69	0.68	-0.59	-0.32	-0.22	-0.22
Peak hip extension (#12)	0.54	0.57	0.71	1.00	0.45	0.53
Peak knee extension in stance (#9)	0.52	0.54	0.77	0.35	0.64	0.55

Max ankle dorsiflexion in stance (#3)	0.47	0.54	0.64	0.40	0.53	0.38
Peak knee flexion in swing (#11)	0.68	0.67	0.70	0.61	0.40	0.27
Ankle dorsiflexion in swing (#7)	0.69	0.75	0.79	0.51	0.58	0.73
Foot clearance (#6)	0.73	0.74	-0.33	0.10	-0.38	0.05
Peak hip flexion (#13)						

Table 5.22 EVGS correlations between scorers (R1, R2) and algorithm for foot position gait set

Parameters	**R1 and R2**		**R1 and algorithm**		**R2 and algorithm**	
	Right	Left	Right	Left	Right	Left
Peak hip flexion (#13)	1.00	1.00	1.00	0.50	1.00	0.50
Knee extension in terminal swing (#10)	0.75	0.75	0.75	1.00	0.72	0.75
Initial contact (#1)	1.00	1.00	1.00	0.92	1.00	0.92
Peak sagittal trunk position (#16)	0.94	0.94	0.80	0.74	0.75	0.81
Pelvic rotation in midstance (#15)	0.77	0.70	0.67	0.52	0.29	0.60
Heel Lift (#2)	0.93	0.93	-0.92	-0.58	-0.94	-0.60
Peak hip extension (#12)	0.80	0.80	1.00	1.00	0.80	0.80
Peak knee extension in stance (#9)	1.00	1.00	0.76	0.89	0.76	0.89
Max ankle dorsiflexion in stance (#3)	0.45	0.45	0.90	0.00	0.43	0.44
Peak knee flexion in swing (#11)	1.00	1.00	0.87	0.94	0.87	0.94
Ankle dorsiflexion in swing (#7)	1.00	1.00	1.00	0.90	1.00	0.90
Foot clearance (#6)	0.76	0.76	-0.22	0.50	-0.22	0.66

Table 5.23 EVGS correlations between scorers (R1, R2) and algorithm for heel lift gait set

Parameters	**R1 and R2**		**R1 and algorithm**		**R2 and algorithm**	
	Right	Left	Right	Left	Right	Left
Peak hip flexion (#13)	0.52	0.76	0.18	0.53	-0.08	0.41
Knee extension in terminal swing (#10)	0.69	0.69	0.23	0.84	0.36	0.76
Initial contact (#1)	0.82	1.00	1.00	0.82	0.82	0.82
Peak sagittal trunk position (#16)	0.67	0.30	0.67	1.00	1.00	0.30
Pelvic rotation in midstance (#15)	0.82	0.82	-0.26	0.22	-0.16	0.27
Heel Lift (#2)	0.90	0.90	-0.69	0.00	0.72	0.05
Peak hip extension (#12)	0.53	0.53	0.36	1.00	0.43	0.53
Peak knee extension in stance (#9)	0.76	0.76	0.90	0.35	0.88	0.23
Max ankle dorsiflexion in stance (#3)	0.55	0.67	0.07	0.68	0.59	0.43

Peak knee flexion in swing (#11)	0.38	0.38	0.36	0.60	-0.26	-0.04
Ankle dorsiflexion in swing (#7)	0.83	0.76	0.54	0.76	0.32	1.00
Foot clearance (#6)	0.67	0.67	-0.27	0.11	-0.41	0.17

Table 5.24 EVGS correlations between scorers (R1, R2) and algorithm for foot clearance gait set

Parameters	**R1 and R2**		**R1 and algorithm**		**R2 and algorithm**	
	Right	Left	Right	Left	Right	Left
Peak hip flexion (#13)	0.76	0.31	0.89	0.59	0.88	0.85
Knee extension in terminal swing (#10)	0.87	0.78	0.10	0.64	-0.12	0.82
Initial contact (#1)	0.63	0.64	0.90	0.92	0.73	0.58
Peak sagittal trunk position (#16)	0.69	0.71	0.69	0.84	0.69	0.85
Pelvic rotation in midstance (#15)	0.08	-0.22	0.24	0.08	-0.20	-0.51
Heel Lift (#2)	0.23	0.21	-0.17	-0.39	-0.43	-0.10
Peak hip extension (#12)	0.29	0.37	0.77	1.00	0.13	0.24
Peak knee extension in stance (#9)	-0.19	-0.15	0.64	-0.19	0.27	0.53
Max ankle dorsiflexion in stance (#3)	0.41	0.51	0.96	0.52	0.55	0.26
Peak knee flexion in swing (#11)	0.65	0.63	0.88	0.27	0.60	-0.09
Ankle dorsiflexion in swing (#7)	0.25	0.49	0.82	-0.15	0.43	0.30
Foot clearance (#6)	0.77	0.81	-0.51	-0.30	-0.52	-0.68

Table 5.25 The overall average correlation between scorers and algorithm, as well as the average correlation of scorers for each parameter.

Parameters	**R1 and R2**	**R1, R2 and Algorithm**		
		Right	Left	Average
Peak hip flexion (#13)	0.81	0.64	0.56	0.60
Knee extension in terminal swing (#10)	0.78	0.65	0.77	0.71
Initial contact (#1)	0.91	0.95	0.90	0.93
Peak sagittal trunk position (#16)	0.83	0.77	0.84	0.81
Pelvic rotation in midstance (#15)	0.68	0.09	0.38	0.23
Heel Lift (#2)	0.80	-0.12	-0.05	-0.09
Peak hip extension (#12)	0.73	0.62	0.79	0.70
Peak knee extension in stance (#9)	0.71	0.78	0.64	0.71
Max ankle dorsiflexion in stance (#3)	0.69	0.64	0.60	0.62
Peak knee flexion in swing (#11)	0.64	0.64	0.58	0.61
Ankle dorsiflexion in swing (#7)	0.83	0.76	0.72	0.74
Foot clearance (#6)	0.67	-0.17	-0.01	-0.09

5.3 Discussion

The discussion is divided into two sub-sections for coronal view parameters and sagittal view parameters. The analysis and conclusions for each parameter are provided at the end of the section.

In each of the two sub-sections, the discussion is structured in the following manner. First, the correlation between scorers is discussed, followed by a discussion on the correlation between scorers and the algorithm. Then, the performance of each parameter for different gait sets is discussed, along with a comparison between the correlation of the scorers and the correlation between the scorers and the algorithm for each parameter.

5.3.1 Coronal view parameters

Based on coronal view analysis across different gait sets, higher correlations among scorers ($r>0.85$) occurred for foot rotation and maximum pelvic obliquity in midstance. Hindfoot valgus and varus had a correlation coefficient of over 0.75, indicating a moderately high level of agreement between scorers. On the other hand, the correlation coefficients were lower for lateral trunk shift and knee progression angle, at less than 0.75. Literature on EVGS interrater reliability found that the level of agreement between scorers varied for each parameter [50]. The highest level of agreement was observed for knee progression angle, with 81% agreement rate among scorers. Foot rotation had a lower agreement rate of 69%, and lateral trunk shift had the lowest agreement rate of 67%. Although there were variations in correlation coefficients in this thesis and level of agreement in the literature, the overall range of agreement among scorers for each gait parameter was consistent between this study and the literature review

Correlations between the algorithm and scorer were highest for foot rotation ($r = 0.77$). However, when considering the intra-scorer reliability mentioned in paper [51], the percentage of agreement between experienced scorers was lower (53%) for foot rotation compared to other parameters. The coorelation for lateral trunk shift was next highest ($r = 0.71$), while hindfoot valgus and varus parameters showed the lowest correlation ($r = -0.03$). Hindfoot valgus/varus correlations were close to zero, indicating no relationship between algorithm and scorer results. Keypoints on the ankle and heel that are near each other in a narrow area and are far from the camera are more likely to be occluded during walking, which helps to explain these differences. Figure **5.3** depicts the change in foot keypoints as the person moves away from the camera. Because the two legs are close together, the foot keypoints for the left leg are not accurately detected. This issue is related

to the smaller size of hindfoot in the video frame, and becoming smaller as the person moves farther from the camera. It is important to note that this challenge is not exclusive to the algorithm because humans may also have difficulties when assessing foot keypoints in similar circumstances.

(a) **(b)**

Figure 5.4 An example where OpenPose fails to recognize heel, ankle, big toe, and small toe accurately.

For pelvic obliquity, the paremeter involves movement of the entire pelvis segment. Hip keypoints were used as a surrogate measure of pelvic movement, since they are a part of the pelvic region. Since these points may not represent the entire pelvic segment, lower correlations between the algorithm and scorer were anticipated. The difference is also attributed to a scorer looking at the entire pelvis when making their assessment, which differs from the algorithm only using hip keypoints.

When analysing parameter correlations for various gait sets, with the exception of the hindfoot valgus and varus parameters, all parameters demonstrated strong correlations between scorers and the algorithm for the healthy gait set. Knee progression angle had a stronger correlation within the knee gait set (participant varied their knee biomechanics while walking), while foot progression angle and lateral trunk shift had the strongest correlation within the foot gait set (participant varied their foot biomechanics while walking).

Figure 5.6 presents the scorer correlation alongside the algorithm/scorer correlation. For all coronal

parameter, correlations between the algorithm and the scorer were lower that between review outcomes. As mentioned in the previous paragraph, this difference can be attributed surrogate measures from OpenPose BODY-25 keypoints. Also, if the camera is not parallel to the coronal plane and oriented vertically, parallax effects may not accurately depict the body segments and orientation can affect measures where the phone axis is assumed to aligned to the ground. This misalignment can result in keypoint detection errors, particularly for body parts that are closer to the camera.

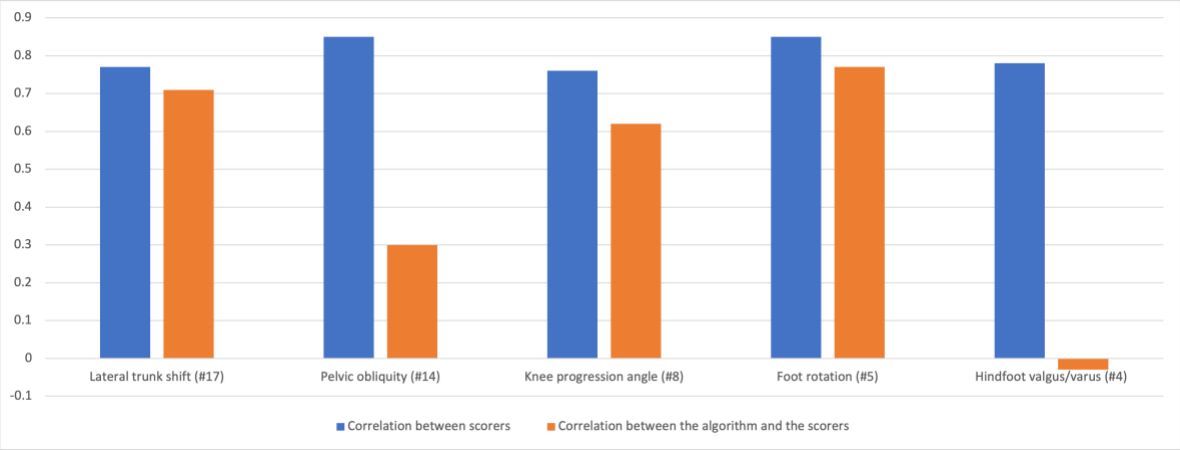

Figure 5.5 Scorer correlation and correlation between the algorithm and the scorers

5.3.2 Sagittal view parameters

Based on the analysis of the data for the sagittal view, it was found that the the level of agreement between scorers was highest for initial contact (r = 0.91), followed by ankle dorsiflexion in swing and trunk position (both 0.83), heel lift (r = 0.80), foot clearance (r = 0.67), and lower for knee flexion (r = 0.64). The literature on interrater reliability of sagittal view gait parameters found that initial contact had an agreement rate of 90%, while foot clearance and heel lift had agreement rates of 82-83% [50] . Knee extension in terminal swing had an agreement rate of 62%, and knee peak flexion in swing had an agreement rate of 69%. In summary, both the thesis results and literature show that initial contact is the most consistent parameter when assessing the interrater reliability of sagittal view gait parameters. Other parameters such as trunk position, ankle dorsiflexion in swing, foot clearance, and heel lift also had high levels of agreement between scorers. However, knee flexion, knee extension in terminal swing, and knee peak flexion in swing had lower levels of agreement.

The correlation between the algorithm and scorer was highest for foot position ($r > 0.85$), followed by trunk position (~0.80), and lowest for heel lift and foot clearance ($r = -0.09$). Foot paramters correlations were close to zero, indicating no relationship between algorithm and scorer results. Foot parameters are a component of smaller joints, are the keypoints farthest from the cameras and are more occluded during walking. Pelvic parameters had lower correlations ($r = 0.23$), which aligns with the percentage of agreement between scorers mentioned in [51] where maximum pelvic obliquity in midstane had a lower agreement rate of 55% compared to other parameters. This lower correlation can be attributed to the use of hip keypoints as a surrogate measure for pelvic movement, as the hips are part of the pelvic region.

Knee flexion and ankle dorsiflexion in swing had stronger correlations between algorithm and scorers when using the foot position gait set. Trunk position had a better correlation for the knee gait set. In contrast, peak hip flexion and ankle dorsiflexion in swing had the strongest correlations when using the ankle gait set.

Figure 5.6 presents the scorer correlation alongside the algorithm/scorer correlation. Except for the heel lift and foot clearance parameters, there is a relationship between the level of agreement among the scorers and the correlation between scorer and algorithmic score of the EVGS. Correlation of the initial contact parameter as assessed by the algorithm and the scorers was higher than the correlation between the scorers themselves. This suggests that the algorithm performs well in accurately assessing the initial contact parameter. There is a substantial difference in the correlation of the peak hip flexion parameter between scorers as well as between the scorers and the algorithm. This variability can be attributed to the fact that the parameter has a definite threshold, where small differences in angle measurements can lead to different scores. For example, a score of 0 corresponds to peak hip flexion angles between 25 º and 45º, while a score of 1 corresponds to angles between 45 º and 60 º. Scorers may not accurately detect small angle changes, such as differences between 44 º and 46 º leading to discrepancies in their assessments. In contrast, the algorithm is able to detect even small changes in angle measurements and assign scores accordingly. Therefore, the algorithm provides a more objective and consistent assessment of the peak hip flexion parameter compared to the subjective assessments of human scorers.

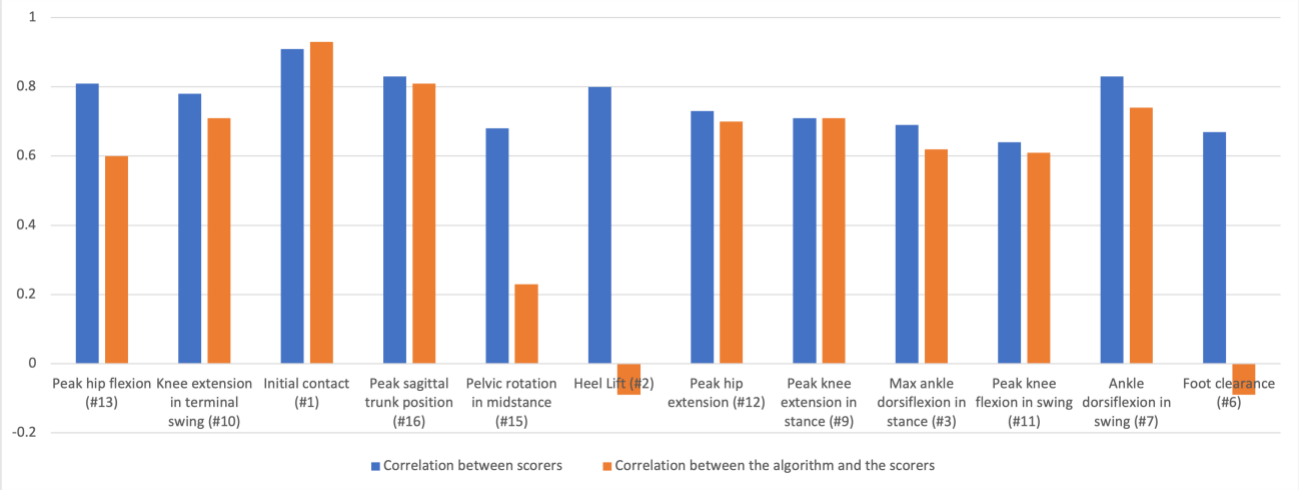

Figure 5.6 Scorer correlation vs the correlation between the algorithm and the scorers

The foot striking and foot off detection are crucial for heel lift. Even a small frame change affects the heel lift parameter. Consider, for instance, a scenario in which the foot strike of the opposite leg occurs at frame 53 and foot off occurs at frame 52. In this case, the patient would be scored as having a normal heel lift (Score 0). The stride detection algorithm identified the foot strike at frame 53 and the foot off at 54. Even if the detected footevent is not accurate, foot event frames still falls within the permitted range of 2, which is used for the stride detection section. The condition would therefore be considered delayed, and a score of one would be assigned. This demonstrates how even a little variation of 1 frame would substantially affect the heel lift parameter.In Figure 5.7(a), the scorers gave the person a score of 2, and the condition was listed as "No clearance." The patient in Figure 5.7(b) obtained a score of 1, and the scorers labeled the condition "Reduced clearance." However, the algorithm recognized Figure 5.7(a) as "Reduced clearance" and Figure 5.7(b) as "No clearance" since the keypoints are clustered in a small area, and there was no data for the floor axis. Therefore, it is anticipated that there would be more inaccuracy in the foot clearance and heel lift parameters.

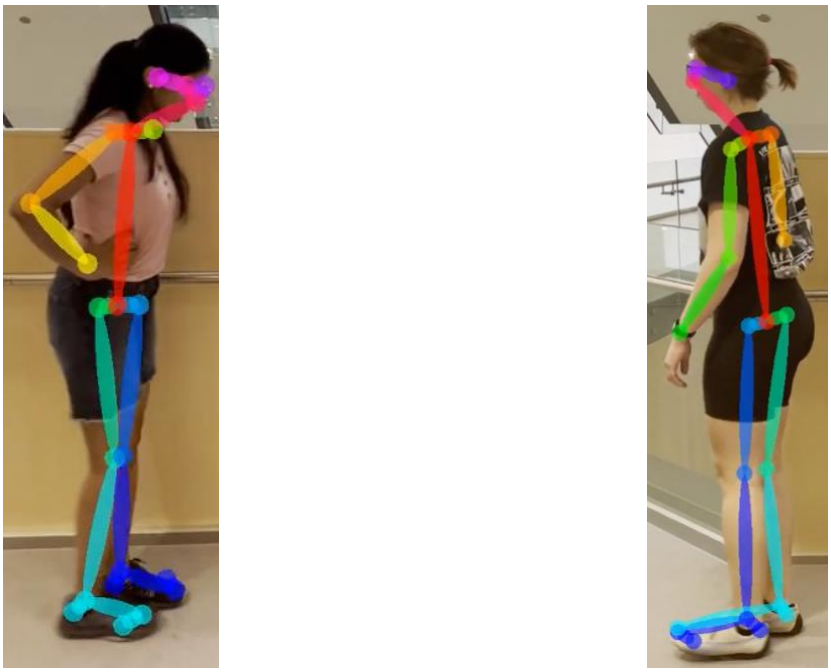

(a) **(b)**

Figure 5.7 (a) No clearance (b) Reduced clearance

5.3.3 Conclusion

The results for each of the various gait parameters included in the EVGS are summarized in the Table 5.26 using the overall average correlation between scorers and algorithm (Table 5.15 and Table 5.25). Correlations were interpreted as very high ($0.9 < r < 1.00$) , high ($0.70 < r < 0.90$), moderate ($0.50 < r < 0.70$), low ($0.30 < r < 0.50$), and negligible ($0.00 < r < 0.30$) [77].

The algorithm performance for identifying gait parameters varied across the different parameters assessed. For foot progression angle (#5), both the correlation between scorers and the correlation between scorers and algorithm were high, indicating that the algorithm performed well in identifying this parameter. The correlation between scorers was also high for this parameter. For knee progression angle (#8), there was moderate agreement between scorers with a correlation of 0.76, while the correlation between scorers and algorithm was 0.62, suggesting that the algorithm performed reasonably well. Finally, for lateral trunk shift (#17), the correlation between scorers was 0.77, indicating moderate agreement, and the correlation between scorers and algorithm was 0.71, suggesting that the algorithm performed reasonably well for this parameter. Pelvic obliquity

(#14) and hindfoot valgus/varus (#4) were two coronal parameters for which the algorithm's performance was relatively poor compared to the human scorers in coronal view. The correlation coefficients between the two scorers were 0.85 for pelvic obliquity and 0.78 for hindfoot valgus/varus. In contrast, the correlation coefficients between the algorithm and each scorer were 0.30 for pelvic obliquity and -0.03 for hindfoot valgus/varus. These results suggest that the algorithm struggled to accurately identify these parameters in a way that aligned with human judgment, particularly for hindfoot valgus/varus. However, it is worth noting that the correlation between the two scorers for hindfoot valgus/varus was relatively low compared to other coronal parameters, which may have contributed to the algorithm's lower performance

The correlation between the algorithm and both scorers for the initial contact parameter was high (0.93). The correlation between the scorers was also high (0.91), suggesting that the algorithm was able to accurately identify the initial contact point in a way that closely aligned with human judgment. This indicates that the algorithm works well for this parameter. For knee extension in terminal swing (#10), peak sagittal trunk position (#16), peak hip extension (#12), peak knee extension in stance (#9), max ankle dorsiflexion in stance (#3), and peak knee flexion in swing (#11), the correlation coefficients between both human scorers and the algorithm were similar and in the same range. This indicates that the algorithm is performing comparably to human scorers for these parameters and is able to identify important gait events in a way that closely aligns with human judgment. The correlation between both scorers for the heel lift parameter (#2) was high (0.80), indicating that they generally agreed on when this gait event occurred. However, the correlation between the algorithm and both scorers was low (-0.09), suggesting that the algorithm had difficulty accurately identifying the heel lift event in a way that aligned with human judgment.

Similarly, for the foot clearance parameter (#6), the correlation between both scorers was moderate (0.67), indicating some variation in their judgments. However, the correlation between the algorithm and both scorers was again low (-0.09).

Table 5.26 Correlation interpretation between scorers (R1 and R2) and algorithm

	Parameter	**Quality**
Coronal Parameters	Foot rotation (#5)	High
	Maximum lateral trunk shift (#17)	High
	Knee progression angle (#8)	Moderate
	Maximum pelvic obliquity in midstance (#14)	Negligible
	Hindfoot valgus/varus (#4)	Negligible
Sagittal Parameters	Initial contact (#1)	Very high
	Peak sagittal trunk position (#16)	High
	Maximum ankle dorsiflexion in swing (#7)	High
	Knee extension in terminal swing (#10)	High
	Peak knee extension in stance (#9)	High
	Peak hip extension in stance (#12)	High
	Maximum ankle dorsiflexion in stance (#3)	Moderate
	Peak knee flexion in swing (#11)	Moderate
	Peak hip flexion in swing (#13)	Moderate
	Pelvic rotation in midstance (#15)	Negligible
	Heel lift (#2)	Negligible
	Foot clearance in swing (#6)	Negligible

6 Summary, Conclusions and Future work

6.1 Research summary

Abnormal gait patterns affect the capacity to carry out daily tasks. Early detection of gait irregularities is essential since it enables strategies to prevent or reduce the effects of these abnormalities on a person's mobility, independence, and overall life quality. The key to enhancing results is early and accurate intervention. Gait analysis is useful in determining normal and pathological gait patterns. The Edinburgh Visual Gait Score (EVGS) is a comprehensive visual assessment tool that is extensively used to help clinicians identify gait patterns. Automating gait analysis using the Edinburgh Visual Gait Scale would offer advantages for both physicians and patients. For physicians, the availability of EVGS data streamlines the decision-making process and enables continuous monitoring of patients. Meanwhile, patients benefit from receiving gait analysis in a local and low-interference setting, saving time and effort on travel and providing more convenient access to healthcare services.

There are three steps involved in automating gait analysis using EVGS:

- A posture estimation model is used to identify joints and body keypoints in a video.
- A stride detection module recognizes the gait strides and foot events.
- Sagittal and coronal parameters are computed using the algorithmic EVGS.

This thesis includes a detailed introduction to stride recognition and visual gait analysis, as well as some major research in this field to aid in developing the foundation necessary for implementing and assessing the study objective. Based on our initial findings, the proposed approach for markerless gait analysis using pose estimation models and automatically evaluating the Edinburgh visual gait scale parameters seems promising. The thesis objective was outlined and result for that is detailed below:

Objective: Design and evaluate an algorithm for detecting foot events and strides, and automatically determine the Edinburgh Visual Gait Scale (EVGS) score from video obtained with a handheld smartphone camera.

An algorithm has been developed for detecting foot events and strides, and automatically determining the Edinburgh Visual Gait Scale (EVGS) score from video obtained with a handheld smartphone camera. To evaluate the feasibility of using the proposed approach for generating

EVGS scores, human scorers were requested to indicate ground truths for foot events and strides and manually score each video using the Edinburgh visual gait scale without any additional analytic tools. Separate validation procedures were used for the stride identification and scoring portions of the Edinburgh visual gait scale.

For the stride detection component, the algorithmically identified foot events are compared with the reviewed ground truth. The comparison revealed that the stride detection component worked better for sagittal videos than coronal videos.

For EVGS component, Of the 17 parameters evaluated using the EVGS, the algorithm produced a correlation coefficient between the two human scorers (R1 and R2) and the algorithm of more than 75 percent for eight parameters. The algorithm provided between 60 and 75 percent correalation results for four parameters, less than 30 percent correalation results for two parameters, and negative correlation results for three parameters (Hindfoot valgus/varus (#4) , Heel lift (#2) , Foot clearance in swing (#6)).

These findings suggest that the use of videos recorded with a handheld smartphone camera, processed by pose estimation models, and assessed by artificial intelligence algorithms is a feasible approach for generating EVGS scores, although further research is needed to improve the algorithm's performance for the parameters with lower correlation coefficients. The results also highlight the importance of human oversight to ensure accurate scoring, particularly for the parameters where the algorithm's performance was limited. However, it should also be noted that the algorithm's output could be better than inexperienced raters.

6.2 Assumptions and limitations

6.2.1 Assumptions

First, it was assumed that the camera held parallel to the plane of movement had minimal movement or shaking while recording the video. Next, it is important that the area where the videos were recorded had appropriate lighting for the algorithm to identify the people. Participants were expected to walk in the targeted area without using mobility aids. Finally, it was assumed that only one participant at a time walked and was recorded on camera and that the results were based on one person at a time.

6.2.1 Limitations

The trials were recorded with a high-end smartphone (iPhone 13 Pro) in a location with good lighting, and there was no person reflection on the wall or floor that the algorithm would mistake for a second person.

To capture all possible EVGS conditions, a healthy person mimicked pathological gait conditions. More research, particularly on patients with pathological gait is needed.

In this study, adult participants were recruited, despite the EVGS scale being designed for children. As a result, there may be size and body ratio differences between adults and the intended population. These differences should be considered when interpreting the study's findings and their applicability to the target age group.

We aim to utilize this system in clinical and patient settings. When deploying this automated EVGS analysis in a patient's home, challenges may arise related to lighting conditions, phone orientation, and the potential misidentification of objects as a person or a person assisting the patient during walking. This thesis did not evaluate various lighting conditions, backgrounds, or several participants at once. Additionally, people using support aids to move, wearing loose clothes, unsteady hand-held video, could negatively affect the results.

6.3 Future work

The thesis created a novel “markerless and clinical scale-based” gait analysis with handheld smartphone data that can deliver results that would be beneficial for both physicians and patients by remotely assessing the patient’s gait with the capacity to be employed in their local environment. This thesis provides an accurate, accessible, and viable technique for automatically assessing human gait using EVGS. The integration of smartphone technology and scale-based gait analysis offers a cost-effective and convenient approach to gait analysis

A potential source of error for the proposed EVGS analysis model is video orientation variability with a hand-held smartphone. Future research could capture smartphone acceleration and orientation data at the same time as recording video, and then use this data to align all video frames to gravity. This would provide a consistent basis for video processing, reducing errors due to varying floor plane angle that affect foot measurements or vertical angle that affects torso and pelvis measurements.

The current sagittal/coronal detection algorithm relies on fixed thresholds, which may not be applicable in all cases. Future work could use ratios or other equations to calculate thresholds that adapt well to different people and environments.

An app for smartphone-based gait analysis can also be created. With the development of a smartphone app for gait analysis, it will be possible to automatically obtain the Edinburgh Visual Gait Score (EVGS) score for a participant simply by capturing a video through the app

Future research should also involve more patient walking data. In each recording session for this experiment, we gathered data on walking for approximately 10 to 15 seconds. For a more accurate capture of the patient's gait pattern, it would be ideal if they provided at least 30 seconds of walking data because the more strides taken, the more foot events that may be recognized, increasing the likelihood that the appropriate score will be determined with the least amount of influence from outliers. People with abnormal gait may require mobility assistance. Future studies should make an attempt to collect as much data as possible from each patient while keeping safety and medical concerns in mind. Additionally, mobility aids as well as varying lighting and ambient conditions need to be considered. To increase the accuracy of the exact identification of frames of the foot events and strides, several ML algorithms may be implemented. In addition to the EVGS, this study may also use other visual gait assessment scales.

7 References

[1] M. W. Whittle, *Gait Analysis: An Introduction*. Butterworth-Heinemann, 2014.

[2] A. Middleton and S. Fritz, "Assessment of Gait, Balance, and Mobility in Older Adults: Considerations for Clinicians," *Curr. Transl. Geriatr. Exp. Gerontol. Rep.*, vol. 2, pp. 205–214, Dec. 2013, doi: 10.1007/s13670-013-0057-2.

[3] R. A. States, J. J. Krzak, Y. Salem, E. M. Godwin, A. W. Bodkin, and M. L. McMulkin, "Instrumented gait analysis for management of gait disorders in children with cerebral palsy: A scoping review," *Gait Posture*, vol. 90, pp. 1–8, Oct. 2021, doi: 10.1016/j.gaitpost.2021.07.009.

[4] T. A. L. Wren, C. A. Tucker, S. A. Rethlefsen, G. E. Gorton, and S. Õunpuu, "Clinical efficacy of instrumented gait analysis: Systematic review 2020 update," *Gait Posture*, vol. 80, pp. 274–279, Jul. 2020, doi: 10.1016/j.gaitpost.2020.05.031.

[5] Z. Cao, G. Hidalgo, T. Simon, S.-E. Wei, and Y. Sheikh, "OpenPose: Realtime Multi-Person 2D Pose Estimation using Part Affinity Fields." arXiv, May 30, 2019. Accessed: Nov. 07, 2022. [Online]. Available: http://arxiv.org/abs/1812.08008

[6] Y. Guo, J. Liu, G. Li, L. Mai, and H. Dong, "Fast and Flexible Human Pose Estimation with HyperPose," 2021, doi: 10.48550/ARXIV.2108.11826.

[7] V. Bazarevsky, I. Grishchenko, K. Raveendran, T. Zhu, F. Zhang, and M. Grundmann, "BlazePose: On-device Real-time Body Pose tracking," 2020, doi: 10.48550/ARXIV.2006.10204.

[8] J. M. Graving *et al.*, "DeepPoseKit, a software toolkit for fast and robust animal pose estimation using deep learning," *eLife*, vol. 8, p. e47994, Oct. 2019, doi: 10.7554/eLife.47994.

[9] J. J. Daly *et al.*, "Development and testing of the Gait Assessment and Intervention Tool (G.A.I.T.): A measure of coordinated gait components," *J. Neurosci. Methods*, vol. 178, no. 2, pp. 334–339, Apr. 2009, doi: 10.1016/j.jneumeth.2008.12.016.

[10] K. A. Hughes and F. Bell, "Visual assessment of hemiplegic gait following stroke: pilot study," *Arch. Phys. Med. Rehabil.*, vol. 75, no. 10, pp. 1100–1107, Oct. 1994, doi: 10.1016/0003-9993(94)90085-X.

[11] W. E. Dickens and M. F. Smith, "Validation of a visual gait assessment scale for children with hemiplegic cerebral palsy," *Gait Posture*, vol. 23, no. 1, pp. 78–82, Jan. 2006, doi: 10.1016/j.gaitpost.2004.12.002.

[12] B. Toro, C. J. Nester, and P. C. Farren, "The Development and Validity of the Salford Gait Tool: An Observation-Based Clinical Gait Assessment Tool," *Arch. Phys. Med. Rehabil.*, vol. 88, no. 3, pp. 321–327, Mar. 2007, doi: 10.1016/j.apmr.2006.12.028.

[13] K. Martin *et al.*, "Development and Reliability of an Observational Gait Analysis Tool for Children with Down Syndrome," *Pediatr. Phys. Ther.*, vol. 21, no. 3, pp. 261–268, 2009, doi: 10.1097/PEP.0b013e3181b13bca.

[14] A. H. Mackey, G. L. Lobb, S. E. Walt, and N. S. Stott, "Reliability and validity of the Observational Gait Scale in children with spastic diplegia," *Dev. Med. Child Neurol.*, vol. 45, no. 1, pp. 4–11, Feb. 2007, doi: 10.1111/j.1469-8749.2003.tb00852.x.

[15] H. S. Read, M. E. Hazlewood, S. J. Hillman, R. J. Prescott, and J. E. Robb, "Edinburgh Visual Gait Score for Use in Cerebral Palsy," *J. Pediatr. Orthop.*, vol. 23, no. 3, 2003, [Online]. Available: https://journals.lww.com/pedorthopaedics/Fulltext/2003/05000/Edinburgh_Visual_Gait_Score_for_Use_in_Cerebral.5.aspx

[16] A. Aroojis, B. Sagade, and S. Chand, "Usability and Reliability of the Edinburgh Visual Gait Score in Children with Spastic Cerebral Palsy Using Smartphone Slow-Motion Video Technology and a Motion Analysis Application: A Pilot Study," *Indian J. Orthop.*, vol. 55, no. 4, pp. 931–938, Aug. 2021, doi: 10.1007/s43465-020-00332-y.

[17] W. Pirker and R. Katzenschlager, "Gait disorders in adults and the elderly: A clinical guide," *Wien. Klin. Wochenschr.*, vol. 129, no. 3–4, pp. 81–95, Feb. 2017, doi: 10.1007/s00508-016-1096-4.

[18] D. M. Wert, J. Brach, S. Perera, and J. M. VanSwearingen, "Gait Biomechanics, Spatial and Temporal Characteristics, and the Energy Cost of Walking in Older Adults With Impaired Mobility," *Phys. Ther.*, vol. 90, no. 7, pp. 977–985, Jul. 2010, doi: 10.2522/ptj.20090316.

[19] D. J. Mayich, A. Novak, D. Vena, T. R. Daniels, and J. W. Brodsky, "Gait Analysis in Orthopedic Foot and Ankle Surgery—Topical Review, Part 1: Principles and Uses of Gait Analysis," *Foot Ankle Int.*, vol. 35, no. 1, pp. 80–90, Jan. 2014, doi: 10.1177/1071100713508394.

[20] H. G. Chambers and D. H. Sutherland, "A Practical Guide to Gait Analysis:," *J. Am. Acad. Orthop. Surg.*, vol. 10, no. 3, pp. 222–231, May 2002, doi: 10.5435/00124635-200205000-00009.

[21] L. M. Silva and N. Stergiou, "The basics of gait analysis," in *Biomechanics and Gait Analysis*, Elsevier, 2020, pp. 225–250. doi: 10.1016/B978-0-12-813372-9.00007-5.

[22] A. Alamdari and V. N. Krovi, "A Review of Computational Musculoskeletal Analysis of Human Lower Extremities," in *Human Modelling for Bio-Inspired Robotics*, Elsevier, 2017, pp. 37–73. doi: 10.1016/B978-0-12-803137-7.00003-3.

[23] A. Nandy, S. Chakraborty, J. Chakraborty, and G. Venture, "Introduction," in *Modern Methods for Affordable Clinical Gait Analysis*, Elsevier, 2021, pp. 1–15. doi: 10.1016/B978-0-323-85245-6.00012-6.

[24] A. Leal-Junior and A. Frizera-Neto, “Gait analysis: overview, trends, and challenges,” in *Optical Fiber Sensors for the Next Generation of Rehabilitation Robotics*, Elsevier, 2022, pp. 53–64. doi: 10.1016/B978-0-32-385952-3.00011-1.

[25] J. B. Webster and B. J. Darter, “Principles of Normal and Pathologic Gait,” in *Atlas of Orthoses and Assistive Devices*, Elsevier, 2019, pp. 49-62.e1. doi: 10.1016/B978-0-323-48323-0.00004-4.

[26] “Gait biomechanics_Range of motion.html.”

[27] A. Bonnefoy-Mazure and S. Armand, “Normal gait,” 2015, pp. 199–214.

[28] K. M. Schweitzer and S. G. Parekh, “Comparison of Gait Biomechanics: Ankle Fusion Versus Ankle Replacement,” *Semin. Arthroplasty*, vol. 21, no. 4, pp. 223–229, Dec. 2010, doi: 10.1053/j.sart.2010.09.003.

[29] C. M. Kawamura, M. C. de Morais Filho, M. M. Barreto, S. K. de Paula Asa, Y. Juliano, and N. F. Novo, “Comparison between visual and three-dimensional gait analysis in patients with spastic diplegic cerebral palsy,” *Gait Posture*, vol. 25, no. 1, pp. 18–24, Jan. 2007, doi: 10.1016/j.gaitpost.2005.12.005.

[30] T. A. L. Wren, G. E. Gorton, S. Õunpuu, and C. A. Tucker, “Efficacy of clinical gait analysis: A systematic review,” *Gait Posture*, vol. 34, no. 2, pp. 149–153, Jun. 2011, doi: 10.1016/j.gaitpost.2011.03.027.

[31] F. M. Chang, A. J. Seidl, K. Muthusamy, A. K. Meininger, and J. J. Carollo, “Effectiveness of Instrumented Gait Analysis in Children With Cerebral PalsyVComparison of Outcomes,” *J Pediatr Orthop*, vol. 26, no. 5, p. 5, 2006.

[32] S. E. Lord, P. W. Halligan, and D. T. Wade, “Visual gait analysis: the development of a clinical assessment and scale,” *Clin. Rehabil.*, vol. 12, no. 2, pp. 107–119, Apr. 1998, doi: 10.1191/026921598666182531.

[33] D. E. Krebs, J. E. Edelstein, and S. Fishman, “Reliability of Observational Kinematic Gait Analysis,” *Phys. Ther.*, vol. 65, no. 7, pp. 1027–1033, Jul. 1985, doi: 10.1093/ptj/65.7.1027.

[34] S. Grunt, P. J. van Kampen, M. M. van der Krogt, M.-A. Brehm, C. A. M. Doorenbosch, and J. G. Becher, “Reproducibility and validity of video screen measurements of gait in children with spastic cerebral palsy,” *Gait Posture*, vol. 31, no. 4, pp. 489–494, Apr. 2010, doi: 10.1016/j.gaitpost.2010.02.006.

[35] A. Harvey and J. W. Gorter, “Video gait analysis for ambulatory children with cerebral palsy: Why, when, where and how!,” *Gait Posture*, vol. 33, no. 3, pp. 501–503, Mar. 2011, doi: 10.1016/j.gaitpost.2010.11.025.

[36] L. A. Koman, J. F. I. Mooney, B. P. Smith, A. Goodman, and T. Mulvaney, “Management of Spasticity in Cerebral Palsy with Botulinum-A Toxin: Report of a Preliminary, Randomized, Double-Blind Trial,” *J. Pediatr. Orthop.*, vol. 14, no. 3, pp. 299–303, Jun. 1994.

[37] C. R. Brown, S. J. Hillman, A. M. Richardson, J. L. Herman, and J. E. Robb, "Reliability and validity of the Visual Gait Assessment Scale for children with hemiplegic cerebral palsy when used by experienced and inexperienced observers," *Gait Posture*, vol. 27, no. 4, pp. 648–652, May 2008, doi: 10.1016/j.gaitpost.2007.08.008.

[38] T. A. L. Wren, S. A. Rethlefsen, B. S. Healy, K. P. Do, S. W. Dennis, and R. M. Kay, "Reliability and Validity of Visual Assessments of Gait Using a Modified Physician Rating Scale for Crouch and Foot Contact:," *J. Pediatr. Orthop.*, vol. 25, no. 5, pp. 646–650, Sep. 2005, doi: 10.1097/01.mph.0000165139.68615.e4.

[39] R. N. Boyd and H. K. Graham, "Objective measurement of clinical findings in the use of botulinum toxin type A for the management of children with cerebral palsy," *Eur. J. Neurol.*, vol. 6, pp. s23–s35, Nov. 1999, doi: 10.1111/j.1468-1331.1999.tb00031.x.

[40] L. A. Koman *et al.*, "Botulinum Toxin Type A Neuromuscular Blockade in the Treatment of Equinus Foot Deformity in Cerebral Palsy: A Multicenter, Open-Label Clinical Trial," *Pediatrics*, vol. 108, no. 5, pp. 1062–1071, Nov. 2001, doi: 10.1542/peds.108.5.1062.

[41] I. S. Corry, A. P. Cosgrove, C. M. Duffy, S. McNeill, T. C. Taylor, and H. K. Graham, "Botulinum Toxin A Compared with Stretching Casts in the Treatment of Spastic Equinus: A Randomised Prospective Trial:," *J. Pediatr. Orthop.*, vol. 18, no. 3, pp. 304–311, May 1998, doi: 10.1097/01241398-199805000-00006.

[42] P. Flett, L. Stern, H. Waddy, T. Connell, J. Seeger, and S. Gibson, "Botulinum toxin A versus fixed cast stretching for dynamic calf tightness in cerebral palsy," *J. Paediatr. Child Health*, vol. 35, no. 1, pp. 71–77, Feb. 1999, doi: 10.1046/j.1440-1754.1999.00330.x.

[43] T. Ubhi, "Randomised double blind placebo controlled trial of the effect of botulinum toxin on walking in cerebral palsy," *Arch. Dis. Child.*, vol. 83, no. 6, pp. 481–487, Dec. 2000, doi: 10.1136/adc.83.6.481.

[44] K. G. B. Maathuis, C. P. van der Schans, A. van Iperen, H. S. Rietman, and J. H. B. Geertzen, "Gait in Children With Cerebral Palsy: Observer Reliability of Physician Rating Scale and Edinburgh Visual Gait Analysis Interval Testing Scale," *J. Pediatr. Orthop.*, vol. 25, no. 3, pp. 268–272, May 2005, doi: 10.1097/01.bpo.0000151061.92850.74.

[45] B. Toro, C. J. Nester, and P. C. Farren, "Inter- and Intraobserver Repeatability of the Salford Gait Tool: An Observation-Based Clinical Gait Assessment Tool," *Arch. Phys. Med. Rehabil.*, vol. 88, no. 3, pp. 328–332, Mar. 2007, doi: 10.1016/j.apmr.2006.12.030.

[46] M. Paci, G. Mini, M. Marchettini, and F. Ferrarello, "The Salford Gait Tool: Does the clinical experience of the raters influence the inter-rater reliability?," *Dev. Neurorehabilitation*, vol. 21, no. 2, pp. 131–132, Feb. 2018, doi: 10.1080/17518423.2016.1247922.

[47] "Reliability and validity of the Observational Gait Scale in children with spastic diplegia.pdf."

[48] L. W. Robinson, N. D. Clement, J. Herman, and M. S. Gaston, “The Edinburgh visual gait score – The minimal clinically important difference,” *Gait Posture*, vol. 53, pp. 25–28, Mar. 2017, doi: 10.1016/j.gaitpost.2016.12.030.

[49] G. P. Bella, N. B. B. Rodrigues, P. J. Valenciano, L. M. A. E. Silva, and R. C. T. Souza, “Correlação entre a Visual Gait Assessment Scale, Edinburgh Visual Gait Scale e Escala Observacional da Marcha em crianças com paralisia cerebral diparética espástica,” *Rev. Bras. Fisioter.*, vol. 16, no. 2, pp. 134–140, Apr. 2012, doi: 10.1590/S1413-35552012000200009.

[50] M. del Pilar Duque Orozco *et al.*, “Reliability and validity of Edinburgh visual gait score as an evaluation tool for children with cerebral palsy,” *Gait Posture*, vol. 49, pp. 14–18, Sep. 2016, doi: 10.1016/j.gaitpost.2016.06.017.

[51] A. M. L. Ong, S. J. Hillman, and J. E. Robb, “Reliability and validity of the Edinburgh Visual Gait Score for cerebral palsy when used by inexperienced observers,” *Gait Posture*, vol. 28, no. 2, pp. 323–326, Aug. 2008, doi: 10.1016/j.gaitpost.2008.01.008.

[52] H. Abe, S. Koyanagi, Y. Kusumoto, and N. Himuro, “Intra-rater and inter-rater reliability, minimal detectable change, and construct validity of the Edinburgh Visual Gait Score in children with cerebral palsy,” *Gait Posture*, vol. 94, pp. 119–123, May 2022, doi: 10.1016/j.gaitpost.2022.03.004.

[53] E. Viehweger *et al.*, “Influence of clinical and gait analysis experience on reliability of observational gait analysis (Edinburgh Gait Score Reliability),” *Ann. Phys. Rehabil. Med.*, vol. 53, no. 9, pp. 535–546, Nov. 2010, doi: 10.1016/j.rehab.2010.09.002.

[54] E. Viehweger, M. Hélix, M. Jacquemier, D. Scavarda, M. A. Rohon, and S. Scorsone-Pagny, “Application of the edinburgh visual gait score: interobserver & intraobserver reliability.,” *Orthop. Proc.*, vol. 87-B, no. SUPP_I, pp. 69–69, Mar. 2005, doi: 10.1302/0301-620X.87BSUPP_I.0870069.

[55] C. Rathinam, A. Bateman, J. Peirson, and J. Skinner, “Observational gait assessment tools in paediatrics – A systematic review,” *Gait Posture*, vol. 40, no. 2, pp. 279–285, Jun. 2014, doi: 10.1016/j.gaitpost.2014.04.187.

[56] M. Moro, G. Marchesi, F. Hesse, F. Odone, and M. Casadio, “Markerless vs. Marker-Based Gait Analysis: A Proof of Concept Study,” *Sensors*, vol. 22, no. 5, p. 2011, Mar. 2022, doi: 10.3390/s22052011.

[57] S. L. Colyer, M. Evans, D. P. Cosker, and A. I. T. Salo, “A Review of the Evolution of Vision-Based Motion Analysis and the Integration of Advanced Computer Vision Methods Towards Developing a Markerless System,” *Sports Med. - Open*, vol. 4, no. 1, p. 24, Dec. 2018, doi: 10.1186/s40798-018-0139-y.

[58] D. Zhang, Y. Wu, M. Guo, and Y. Chen, “Deep Learning Methods for 3D Human Pose Estimation under Different Supervision Paradigms: A Survey,” *Electronics*, vol. 10, no. 18, Art. no. 18, Jan. 2021, doi: 10.3390/electronics10182267.

[59] G. Ning, P. Liu, X. Fan, and C. Zhang, "A Top-Down Approach to Articulated Human Pose Estimation and Tracking," in *Computer Vision – ECCV 2018 Workshops*, L. Leal-Taixé and S. Roth, Eds., in Lecture Notes in Computer Science, vol. 11130. Cham: Springer International Publishing, 2019, pp. 227–234. doi: 10.1007/978-3-030-11012-3_20.

[60] T. D. Nguyen and M. Kresovic, "A survey of top-down approaches for human pose estimation," 2022, doi: 10.48550/ARXIV.2202.02656.

[61] M. Li, Z. Zhou, J. Li, and X. Liu, "Bottom-up Pose Estimation of Multiple Person with Bounding Box Constraint." arXiv, Jul. 26, 2018. Accessed: Dec. 05, 2022. [Online]. Available: http://arxiv.org/abs/1807.09972

[62] A. Mathis *et al.*, "DeepLabCut: markerless pose estimation of user-defined body parts with deep learning," *Nat. Neurosci.*, vol. 21, no. 9, pp. 1281–1289, Sep. 2018, doi: 10.1038/s41593-018-0209-y.

[63] G. Papandreou, T. Zhu, L.-C. Chen, S. Gidaris, J. Tompson, and K. Murphy, "PersonLab: Person Pose Estimation and Instance Segmentation with a Bottom-Up, Part-Based, Geometric Embedding Model." arXiv, Mar. 22, 2018. Accessed: Dec. 13, 2022. [Online]. Available: http://arxiv.org/abs/1803.08225

[64] A. Toshev and C. Szegedy, "DeepPose: Human Pose Estimation via Deep Neural Networks," 2013, doi: 10.48550/ARXIV.1312.4659.

[65] E. Insafutdinov, L. Pishchulin, B. Andres, M. Andriluka, and B. Schiele, "DeeperCut: A Deeper, Stronger, and Faster Multi-Person Pose Estimation Model," 2016, doi: 10.48550/ARXIV.1605.03170.

[66] H.-S. Fang *et al.*, "AlphaPose: Whole-Body Regional Multi-Person Pose Estimation and Tracking in Real-Time," 2022, doi: 10.48550/ARXIV.2211.03375.

[67] F. Zhang *et al.*, "Comparison of OpenPose and HyperPose artificial intelligence models for analysis of hand-held smartphone videos," in *2021 IEEE International Symposium on Medical Measurements and Applications (MeMeA)*, Lausanne, Switzerland: IEEE, Jun. 2021, pp. 1–6. doi: 10.1109/MeMeA52024.2021.9478740.

[68] S. Mroz *et al.*, "Comparing the Quality of Human Pose Estimation with BlazePose or OpenPose," in *2021 4th International Conference on Bio-Engineering for Smart Technologies (BioSMART)*, Paris / Créteil, France: IEEE, Dec. 2021, pp. 1–4. doi: 10.1109/BioSMART54244.2021.9677850.

[69] E. D'Antonio, J. Taborri, E. Palermo, S. Rossi, and F. Patane, "A markerless system for gait analysis based on OpenPose library," in *2020 IEEE International Instrumentation and Measurement Technology Conference (I2MTC)*, Dubrovnik, Croatia: IEEE, May 2020, pp. 1–6. doi: 10.1109/I2MTC43012.2020.9128918.

[70] J.-H. Yoo and M. S. Nixon, “Automated Markerless Analysis of Human Gait Motion for Recognition and Classification,” *ETRI J.*, vol. 33, no. 2, pp. 259–266, 2011, doi: 10.4218/etrij.11.1510.0068.

[71] A. H. Myriam, G. Salim, E. David, and K. Mohammad, “An automated method for analysis of gait data to aid clinical interpretation,” in *2011 1st Middle East Conference on Biomedical Engineering*, Feb. 2011, pp. 119–121. doi: 10.1109/MECBME.2011.5752079.

[72] A. Viswakumar, V. Rajagopalan, T. Ray, and C. Parimi, “Human Gait Analysis Using OpenPose,” in *2019 Fifth International Conference on Image Information Processing (ICIIP)*, Nov. 2019, pp. 310–314. doi: 10.1109/ICIIP47207.2019.8985781.

[73] H. S. Read, M. E. Hazlewood, S. J. Hillman, R. J. Prescott, and J. E. Robb, “Edinburgh Visual Gait Score for Use in Cerebral Palsy:,” *J. Pediatr. Orthop.*, vol. 23, no. 3, pp. 296–301, May 2003, doi: 10.1097/01241398-200305000-00005.

[74] I. W. Selesnick and C. S. Burrus, “Generalized digital Butterworth filter design,” *IEEE Trans. Signal Process.*, vol. 46, no. 6, pp. 1688–1694, Jun. 1998, doi: 10.1109/78.678493.

[75] C. J. C. McGuirk, N. Baddour, and E. D. Lemaire, “Video-Based Deep Learning Approach for 3D Human Movement Analysis in Institutional Hallways: A Smart Hallway,” *Computation*, vol. 9, no. 12, Art. no. 12, Dec. 2021, doi: 10.3390/computation9120130.

[76] J. Zeni, J. Richards, and J. Higginson, “Two simple methods for determining gait events during treadmill and overground walking using kinematic data,” *Gait Posture*, vol. 27, pp. 710–4, Jun. 2008, doi: 10.1016/j.gaitpost.2007.07.007.

[77] M. Mukaka, “A guide to appropriate use of Correlation coefficient in medical research,” *Malawi Med. J. J. Med. Assoc. Malawi*, vol. 24, no. 3, pp. 69–71, Sep. 2012.

Appendix A: Research Ethics Board Approval Certificate

01/03/2023

Université d'Ottawa
Bureau d'éthique et d'intégrité de la recherche

University of Ottawa
Office of Research Ethics and Integrity

CERTIFICAT D'APPROBATION ÉTHIQUE | CERTIFICATE OF ETHICS APPROVAL

Numéro du dossier / Ethics File Number	H-02-23-8945
Titre du projet / Project Title	Artificial Intelligence implementation of Edinburgh Visual Gait Score (EVGS)
Type de projet / Project Type	Thèse de maîtrise / Master's thesis
Statut du projet / Project Status	Approuvé / Approved
Date d'approbation (jj/mm/aaaa) / Approval Date (dd/mm/yyyy)	01/03/2023
Date d'expiration (jj/mm/aaaa) / Expiry Date (dd/mm/yyyy)	28/02/2024

Équipe de recherche / Research Team

Chercheur / Researcher	Affiliation	Role
Shri Harini RAMESH	Département de génie mécanique / Department of Mechanical Engineering	Chercheur Principal / Principal Investigator
Natalie BADDOUR	Département de génie mécanique / Department of Mechanical Engineering	Superviseur / Supervisor
Edward LEMAIRE	Département de médecine / Department of Medicine	Co-superviseur / Co-supervisor

Conditions spéciales ou commentaires / Special conditions or comments

550, rue Cumberland, pièce 154
Ottawa (Ontario) K1N 6N5 Canada

550 Cumberland Street, Room 154
Ottawa, Ontario K1N 6N5 Canada

613-562-5387 • 613-562-5338 • ethique@uOttawa.ca / ethics@uOttawa.ca
www.recherche.uottawa.ca/deontologie | www.recherche.uottawa.ca/ethics